UNIVERSIDADE DO ALGARVE
FACULDADE DE CIÊNCIAS E TECNOLOGIA
2018

CO_2 flux variability in the Galician Upwelling System

Author: Laura Pacho

Supervisors: Xosé Antonio Padín and Alexandra Cravo

Final Master Thesis with the Marine Research Institute of Vigo and the University of Algarve

Faro 28/09/2018

Declaration of authorship of work

I declare to be the author of this work, which is original and unpublished. Authors and works consulted are duly cited in the text and are included in the list of references.

Declaro ser a autora deste trabalho, que é original e inédito. Autores e trabalhos consultados estão devidamente citados no texto e constam da listagem de referências incluída.

Copyright

Acknowledgment

I would like first to thank the Marine Research Institute in Vigo for the opportunity to be part of this project. Thank you Xosé Antonio Padín and Fiz Fernández Pérez for giving me support with my data and corrections and I would like to thank the people from the Oceanography Department, from in the Marine Research Institute of Vigo, who helped me enormously, giving me support or help when I needed.

I would like to thank my co-supervisor Alexandra Cravo from the University of Algarve, who helped me in each step giving me support with my work and help when I have issues with this travel.

I would like to thank all the people who always encourage me to keep trying, friends and family, and especially to my colleagues from the Master who even in the distance always were ready with an answer, and finally, I would like to thank Sara and Elisabeth, who were very supportive in the most stressing moments during my stay in Vigo.

Thank you.

INDEX

INDEX: FIGURES

INDEX: TABLES

RESUMO

Embora os ecossistemas costeiros sejam componentes importantes do ciclo de carbono global, seu papel como sumidouros ou fontes de CO_2 não é bem definido devido à forte heterogeneidade espacial, variabilidade temporal e à relativa escassez de dados. Os fluxos de carbono podem mudar rapidamente, e como tal as estimativas dos fluxos de CO_2 entre o oceano e a atmosfera estão sujeitas a grandes incertezas.

O afloramento costeiro ocorre ao longo das margens oceânicas orientais (EBUS), nas quatro principais regiões Oceano Mundial são: Califórnia, Canárias, Benguela e Peru / Humboldt. O afloramento costeiro induzido pelo transporte de Ekman promove o aumento de nutrientes e CO_2 na zona eufótica dos oceanos. EBUS podem ser fontes ou sumidouros de CO_2 para a atmosfera, dependendo da intensidade do evento de afloramento ou do tempo de permanência das águas ressurgidas sobre a plataforma continental. Processos biológicos desempenham um papel crucial na determinação do pCO2 na superfície do mar, nessas áreas.

No entanto, face às mudanças climáticas é dificil conhecer com rigor como esses sistemas de afloramento costeiro se comportarão nos próximos anos. Nesse contexto, Bakun, em 1973, publicou uma teoria com base no aumento substancial de CO_2 e outros gases de efeito estufa na atmosfera, o que criará uma diminuição do arrefecimento durante a noite, o que desenvolverá uma intensificação de aquecimento na zona continental adjacente às regiões de afloramento. Para este autor, o vento ao longo da costa que impulsiona o afloramento costeira será mantido em parte por um forte gradiente de pressão atmosférica desenvolvido sobre a massa terrestre aquecida e a maior pressão barométrica sobre o oceano mais frio. Cientistas de todo o mundo estão tentando testar essa hipótese, apesar de existirem algumas contradições entre eles.

Apesar das semelhanças físicas dos EBUS cada um tem características particulares e, portanto, são diferentes de várias maneiras. Na costa da Galiza, que está localizada no limite norte do sistema de afloramento das Canárias, na parte subtropical do Atlântico Norte, o padrão de afloramento é caracterizado por uma forte sazonalidade. O litoral da Galiza caracteriza-se principalmente pela presença das Rías Baixas, quatro grandes enseadas costeiras (> 2,5 km^3) entre 42ºN e 43ºN. A troca de água entre as Rias Baixas

e as águas de largo é drasticamente afetada pelo padrão de vento costeiro. Eventos de afloramento são comumente observados durante a primavera-verão devido à predominância de ventos de nordeste. O transporte de Ekman zonal na costa das águas superficiais é denominado Eastern North Atlantica Central Waters (ENACW).

Existem poucos estudos com séries temporais longas e grandes escalas espaciais, os quais que poderiam ajudar a avaliar as conseqüências e fornecer conclusões sobre como mudanças climáticas afetarão esse tipo de processo. Neste contexto, este projecto visa contribuir para o aumento deste conhecimento e centrar-se-á na Ria de Vigo, onde os ventos são os principais responsáveis pelas alterações observadas na hidrografia, e estas alterações estão também associadas ao padrão de circulação residual de duas camadas, característica dos estuários parcialmente misturados.

O afloramento costeiro da Ria de Vigo actua como sumidouro líquido de CO_2 o que está relacionado com as elevadas taxas de descarga ea exaustão de nutrientes, que causam uma subsaturação de CO_2 mais intensa e variável na plataforma do que no mar ou nas Rias Baixas, onde são observadas intensas emissões de CO_2 durante o outono.

Neste trabalho investigou-se a variabilidade dos fluxos de CO_2 à superfície no sistema de afloramento da Galiza, a partir de dados recolhidos pelo Instituto de Investigações Marinhas em Vigo, no período de 1997 a 2018. Para tal, relacionou-se a sua sazonalidade com a variabilidade de alterações em ambos os componentes físicos, como temperatura superficial (SST), salinidade superficial (SSS) e upwelling (I_w), e biológico por clorofila a (Chl*a*) e a Produção Líquida do Ecossitema (NEP).

Para tal estimaram-se os fluxos anuais de CO_2 e o índice de afloramento na Galiza, a partir de dados que incluem a pressão parcial de CO_2 à superfície do mar (pCO_2^{sw}), temperatura superfícial do mar (SST) e salinidade superfícial do mar (SSS), velocidade do vento (NCEP / NCAR e CCMP), Chla e NEP (SeaWiFS e MODIS). Existem poucos estudos com séries temporais longas e este trabalho pode fornecer respostas sobre como as diferentes variáveis mudam devido ao aumento dos gases de efeito estufa.

Os resultados mostraram que a tendência da velocidade do vento durante a primavera e o verão foi de diminuir de 1997 a 2018, contrariamente ao proposto pela teoria de Bakun. Embora não seja possível determinar uma tendência de queda do índice de afloramento, é verdade que os valores máximos de 1997 a 2018 diminuíram em relação

aos estudados entre 1997 e 2009. O fCO_2^{sw} tem dois componentes principais que definem seu comportamento, que são o componente biológico, relacionado com a fotossíntese e os processos heterotróficos, e o componente físico da temperatura que entra em jogo na troca de temperaturas maiores durante o verão em contraste com as mais frias no inverno. Neste caso os processos de origem biológica tiveram mais peso durante a maior parte do ano marcado por processos de fotossíntese e, portanto, de absorção de CO_2 durante a Primavera e o Verão, enquanto que durante o inverno o componente biológico parece indicar processos heterotróficos. Este é o caso, exceto em épocas de maior índice de troca de temperatura quando,durante os meses do final do verão e início do outono as aguas estão mais quentes, dependendo da zona e pasam a ser mais frias (dentro do estuario ou fora), quando a componente físico da temperatura se sobrepõe ao componente biológico.

Dentro da Ria, a sazonalidade e os efeitos do afloramento são muito mais fortes do que no caso dos processos ao largo, tendo também a Ria uma importante influência da componente proveniente das águas continentais. A Oscilação do Atlântico Norte está relacionada com a SST e ΔfCO_2, o que é importante para se estudarem os ciclos inter-anuais. No entanto neste trabalho não existiu um componente cíclico inter-anual para a fCO_2^{sw}.

É importante continuar a analisar e aumentar as bases de dados para determinar de que forma essas variáveis continuam a evoluir face aos desafios que a própria mudança climática proporciona.

Palavras chave: Dióxido de carbono, afloramento costeira, troca ar-mar de CO_2, aquecimento global.

ABSTRACT

Coastal upwelling occurring along the eastern ocean margins (EBUS), at the four major eastern boundary current regions of the World Ocean: California, Canary, Benguela, and Peru/Humboldt, induces offshore surface Ekman Transport and promotes the rise of deep nutrient and CO_2-rich water into the euphotic zone. However, how these coastal upwelling systems will behave next years due to climate change, its something that scientists do not understand yet perfectly well. Within this context, Bakun in 1973 published a theory explaining why climate change will promote an intensification of upwelling. Scientists around the world are trying to test this hypothesis despite some contradictions exist between them. The objective of this work was to approach this topic studying Galician upwelling system using data collected between 1997 and 2018 by the Marine Research Institute in Vigo, España. The database included CO_2 partial pressure at sea surface (pCO_2^{sw}), sea surface temperature (SST) and sea surface salinity (SSS), Wind Speed (NCEP/NCAR) and (CCMP), Chla and NEP (SeaWiFS and MODIS). The results showed that the tendency of wind speed during Spring and Summer is to decrease from 1997 to 2018, contrary to that stated by Bakun. Although it is not possible to establish a downward trend of the upwelling index, it is true that the maximum values from 1997 to 2018 have decreased with respect to those achieved from 1997 to 2009. fCO_2^{sw} has two main components that define its behavior, which are the biological component, related to photosynthesis and heterotrophic processes, and the physical component of temperature that comes into play at times of maximum upwelling index. Within the Ria de Vigo seasonality and the effects of upwelling are much stronger than offshore. Moreover, there the contribution from the continental waters areimportant . The North Atlantic Oscillation is related to SST and to ΔfCO_2, which is important at the time of looming interannual cycles, although in this work there is no high inter-annual cyclical component for fCO_2^{sw}.

Key words: Carbon dioxide, Coastal Upwelling, CO_2 air-sea exhange, Climate Change.

LIST OF ACRONYMS

EBUS: Eastern Boundary Upwelling Systems.

ENAUS: Eastern North Atlantic Upwelling System.

ENAW: Eastern North Atlantic Water.

NAO: North Atlantic Oscillation.

NEP: Net Ecosystem Production.

Chl *a*: Chlorophyll *a*.

SST: Sea Surface Temperature.

SSS: Sea Surface Salinity.

PAR: Photosynthetically active radiation.

VGPM: Vertically Generalized Production Model.

CCMP: Cross-Calibrated Multi-Platform.

SeaWiFs: Sea-Viewing Wide Field of View Sensor.

MODIS: Moderate Resolution Imaging Spectroradiometer.

CTD: Conductivity, Temperature and Depth.

LIST OF SYMBOLS

pCO_2^{atm}: Partial pressure of CO_2 in the atmosphere.

pCO_2^{sw}: Partial pressure of CO_2 in seawater.

pH_2O: Partial pressure of water.

fCO_2^{atm}: Fugacity in the atmosphere.

fCO_2^{sw}: Fugacity in seawater.

${}^{B}fCO_2^{sw}$: Biological component of fugacity in seawater.

${}^{T}fCO_2^{sw}$: Temperature component of fugacity in seawater.

FCO_2: CO_2 flux air-sea exchange.

I_w: Upwelling Index.

k: Gas Transfer Velocity.

A_T:Total alkalinity

1. INTRODUCTION

1.1 THE EASTERN BOUNDARY UPWELLING SYSTEMS (EBUS)

Coastal upwelling is an important oceanographic process that supports some of the most productive regions of the ocean (Barton *et al*., 2013). The estimations point that 18–33% of the global net primary production and 27–50% of the global export production occur in upwelling regions. Moreover, 90% of the world's fisheries occur in 2-3% of the oceans, mostly correspondent to coastal upwelling systems (Pond & Pickard, 2016), although ocean margins cover only 8% of the total ocean surface *(Álvarez-Salgado et al*., 2001). These high productive areas support a large net fixation of CO_2 by phytoplankton and subsequent export of organic carbon, which compensates the CO_2 coming with the upwelled cold waters (Lachkar and Gruber, 2013).

Upwelling is developed by wind stress which induces offshore surface Ekman Transport and promotes the rise of deep nutrient and CO_2-rich water (Perez *et al*., 2010; Lachkar and Gruber, 2013). This water derives from depths not greater than 200-300 m (Pond & Pickard, 2016) to the euphotic zone near the coast, stimulating high phytoplankton growth (Perez *et al*., 2010; Lachkar and Gruber, 2013). However, not all subsurface waters have a high concentration of nutrients, which means that upwelling does not promote always this biological production (Pond & Pickard, 2016).

Coastal upwelling plays an important role in the air-sea exchange of CO_2 and has also a profound effect on local climate characteristics (Narayan *et al*., 2010). The upwelling events can last 3-10 days, and sometimes more than 14 days (García-Reyes *et al*., 2014). There are three main requirements to increase productivity in these upwelling systems, two of them, physical processes: (1) more important nitrate concentration, and the thermocline that, must be shallow, located in the depth range of 40–80 m or less ;(2) upwelling-favorable winds can provide nutrient-rich waters into the photic zone, stimulating photosynthesis; and (3) iron derived from external sources like a river incoming to the system (Chavez *et al*., 2002).

Coastal upwelling develops at the four major eastern boundary systems (EBUS) around the World Ocean: California, Peru/Humboldt, Benguela and Canary *(*Álvarez-Salgado *et al*., 2000) (Fig. 1.1). The Canary Current ranges 12-43°N and are distinguished by a strong geographical diversity. This fact can determine the unique upwelling ecosystem

response of the different areas embedded in the Canary Current (Arístegui *et al*., 2009). The Canary Upwelling system will be studied in this project, particularly in the region of the Rias Baixas, in the NW Coast of Spain.

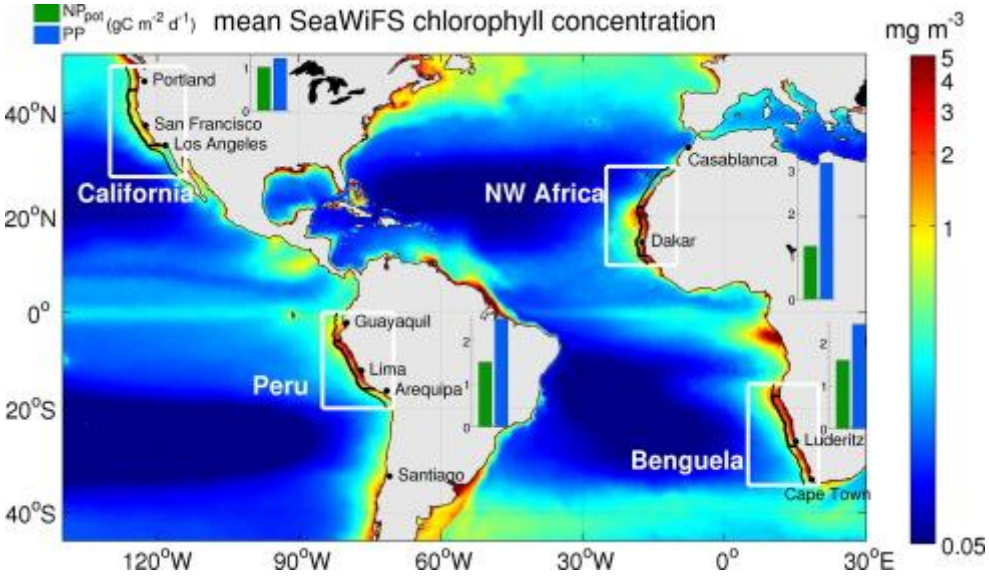

Figure 1.1: Location of EBUS in the world (Messié and Chavez, 2015).

1.2 THE RÍAS BAIXAS AND COASTAL UPWELLING

The Rías Baixas are constituted by four coastal embayments (>25 km^3) on the western coast of Galicia (NW Spain), Ría de Muros and Noia, Ria de Arousa, Ría de Pontevedra and Ría de Vigo (Álvarez-Salgado et al., 1993) (Fig. 1.2), situated in the northernmost limit of the Eastern North Atlantic Upwelling System (ENAUS), a branch of the Canary Upwelling system (Alvarez *et al*., 2009). At the latitudes of the Rías Baixas, upwelling events result in the movement of Eastern North Atlantic Waters (ENAW), across the shelf coming into the Rías along the bottom (Fig. 1.3) (Álvarez-Salgado *et al*., 1993).

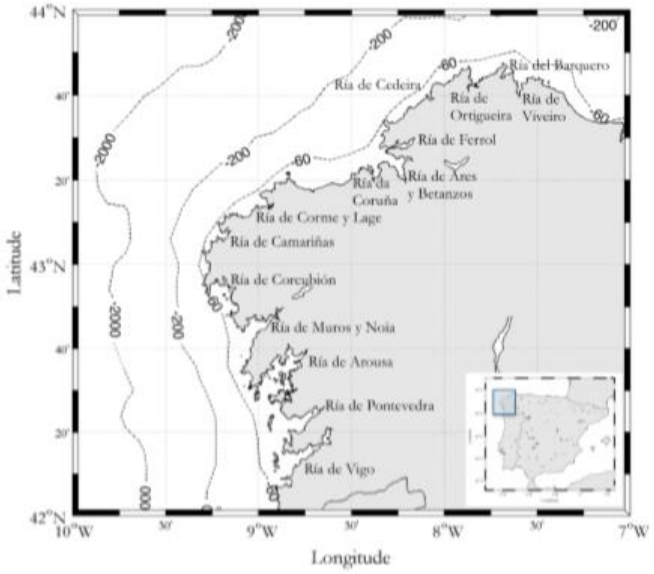

Figure 1.2: Location of the Rías Baixas.

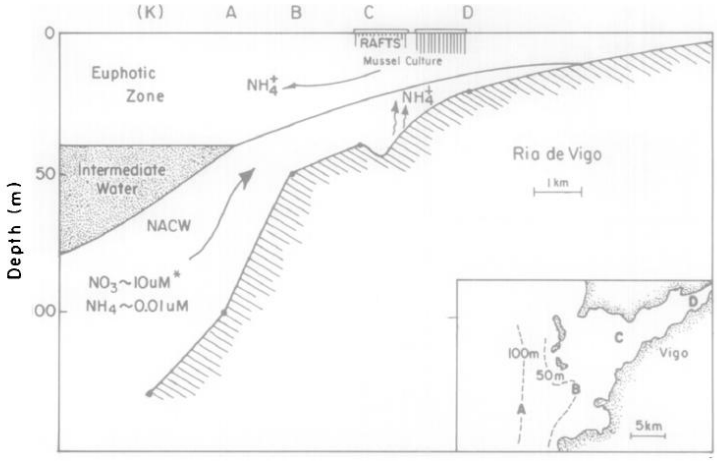

Figure 1.3: Upwelling, NACW (North Atlantic Central Water) (Fraga, 1988).

At the Rías Baixas, upwelling occurs more frequently from April to September due to the predominance of northerly winds (Blanton *et al*., 1987). However, there are authors reporting longer upwelling periods, from March–April to September–October (Alvarez *et al*., 2009). Coastal upwelling has also been observed even in autumn-winter under some specific wind conditions as it occurred in January 1998, when there was pumping of seawater from the Iberian Poleward Current into the Ría de Pontevedra (Alvarez *et al*., 2009). Upwelling/relaxation cycles as a result of these coastal winds occur with a periodicity of 10 to 20 days during the upwelling season (Álvarez-Salgado *et al*., 2002).

During winter, southerly winds appear forcing the coastal downwelling in the superficial waters, under the influence of the Iberian Poleward Current (Alvarez *et al*.,

2009). Furthermore, the run-off of the rivers contributes to the presence of river plumes over the shelf which varied rapidly according to wind stress (Cobo-Viveros *et al*., 2013). Part of the biomass produced in the Rías is exported to the shelf by these river plumes, and together with this downwelling front, the biomass will reach the bottom layer over the shelf where remineralization takes place. The downwelling will provoke homogenization of the water leaving the biomass in the bottom. Sometimes when there is less solar radiation, the biomass levels are low. In the frontal zone of the Ria where the proper dynamic of recirculation and sink zones of the Ria accumulates biomass, where the local gradient of salinity is higher (Álvarez-Salgado *et al*., 1993; (Nogueira *et al*., 2000; Gago *et al*., 2003).

The intensity of the seasonal upwelling and downwelling in this region varies strongly between different years (Arístegui *et al*., 2006), describing decadal cycles linked to NAO (Hurrell, 1995).

This project will be focused in Ría de Vigo where winds are mainly responsible for the changes observed in the hydrography, and these changes are also associated with the two-layered residual circulation pattern which is characteristic of partially mixed estuaries (Diz *et al*., 2006). It is considered a partially mixed estuary because it is forced by wind stress as coastal upwelling systems and not by continental runoff as commonly found in mixed estuaries (Doval *et al*., 2016). The positive residual circulation is the inflow through the bottom layer and outflow through the surface layer, happening under the influence of northerly winds. When there is a reversal of winds, under southerlies the inflow will be through the surface layer and the outflow through the bottom layer (Diz *et al*., 2006).

The unique combination of wind patterns and coastal morphology makes the Rías Baixas a highly productive system, where frequent upwelling events occur, promoting an enrichment of nutrients and availability of CO_2, an exceptional site for the extensive culture of the blue mussel *Mytilus galloprovincialis.* It represents one of the major shared world markets of blue mussels, with a total production of about 250,000 tons per year, representing 40% of European, and 15% of the world production (Álvarez-Salgado *et al*., 2008).

1.2.1 CO_2 in the upwelling regions and at the Rías Baixas

Under upwelling events, pCO_2 supersaturated waters are brought to the surface to the coast of EBUS (Borges and Frankignoulle, 2001), playing an important role in the air-sea exchange of CO_2 (Álvarez-Salgado *et al*., 2002). Nevertheless, these air-sea exchanges are particularly complex (Fig. 1.4), as a result from processes that have antagonistic effects on the surface seawater partial pressure of CO_2 (pCO_2) values (Borges and Frankignoulle, 2001; Borges *et al*., 2005). Several recent articles reporting global estuarine and coastal ocean CO_2 fluxes concluded that although the global estuarine and coastal area is very small, this CO_2 degassing flux is as large as the CO_2 uptake by the continental shelf and that both flux terms are significant in the global CO_2 flux (Cai, 2011).

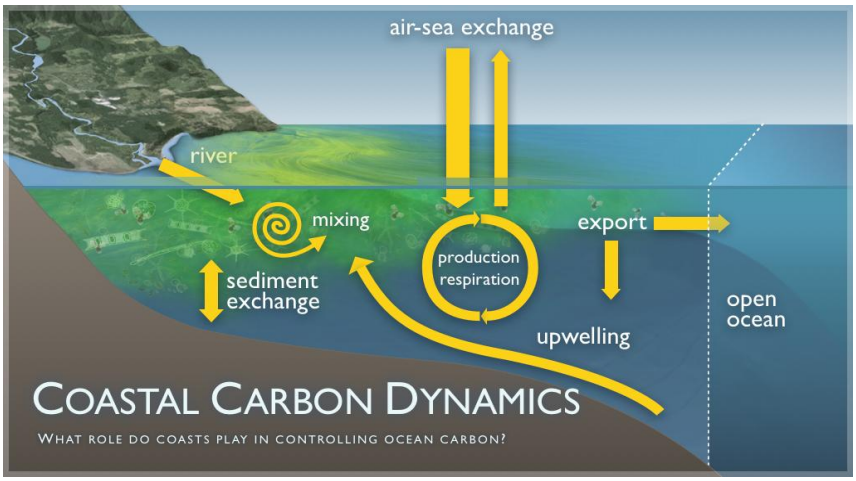

Figure 1.4: CO_2 cycle air-sea exchange (Team, 2018).

The great number of uncertainties to predict CO_2 changes air-sea water exchange, in the role of the continental shelf seas depends on the availability of CO_2 data in spatial and temporal scales (Cobo-Viveros *et al*., 2013). Although several studies have deal with the fCO_2^{sw} in surface waters in the coastal zone, there has been little emphasis on upwelling regions. As there, biological productivity can be very high, fCO_2^{sw} can be rapidly reduced (Gago *et al*., 2003). Some authors report that biological processes in some places can be as important as changes in temperature (Simpson and Zrino, 1980). In general, the available data sets do not fully cover the annual cycle. So, it is unclear if upwelling systems behave as sinks or sources of atmospheric CO_2 (Borges and Frankignoulle, 2002).

Studies agree that the NW Iberian upwelling system behaves as a sink for atmospheric CO_2 (Pérez *et al*., 1999). The high absorption rates are due to the relatively low pCO_2 levels of the upwelled waters, compared with aged central waters of the coastal upwelling regions that act as sources of CO_2 to the atmosphere, and due to the intermittency of the NW Iberian upwelling. This fact allows for an efficient utilization of upwelled CO_2 and nutrients that increase primary production, comparable with other coastal upwelling systems where the nutrient input is much higher (Arístegui *et al*., 2006).

1.3 CARBON DIOXIDE IN THE OCEAN AND AIR-SEA CO_2 EXCHANGE: CARBON MEASUREMENTS

The direct atmospheric measurements began 1958 by analyzing air enclosed in polar ice with ice core measurements (Etheridge *et al*., 1996). In recent years due to climate changes and the concern about the rise of CO_2 levels, there is an urgency to study the CO_2 seawater exchange.

The increase of atmospheric levels of CO_2 accounts for about 60% of the CO_2 emitted by fossil fuel sources (Wanninkhof *et al*., 2009). The seasonal cycle of CO_2 atmospheric molar fraction (xCO_2^{atm}), is the result of a combination of uptake and release by plant and soils and seasonally by oceanic waters and anthropogenic emission (Padin *et al*., 2007). The gas exchange contributes to the migrations of the greenhouse anthropogenic gases through the absorption by the oceans of the excess of CO_2 (Wanninkhof *et al*., 2009). The ocean uptakes CO_2 from the atmosphere within the range of 17–39% of the fossil fuel emissions (Siegenthaler and Sarmiento, 1993).

In the water, there are different forms of carbon, the form the total dissolved inorganic carbon (Eq. 1):

$$C_T = CO_2(dissolved) + H_2CO_3 + HCO_3^- + CO_3^{2-} \quad \text{(Equation 1)}$$

The global mean total carbon in deep waters below 1200 m is higher than in surface mixed layers. So, it is important to understand how this carbon cycle works in between the ocean and the atmosphere (Legendre *et al*., 2015). The carbonate system is expressed in the following reactions (Eq. 2):

$$CO_2 + H_2O \overset{K1}{\leftrightarrow} HCO_3^- + H^+ \overset{K2}{\leftrightarrow} CO_3^{2-} + 2H^+ \quad \text{(Equation 2)}$$

The carbonate pump also creates a vertical gradient in total alkalinity (Eq. 3) (Legendre *et al*., 2015):

$$A_T = [HCO_3^-] + 2[CO_3^{2-}] + [B(OH)_4^-] + [OH^-] - [H^+] + \ minor\ compounds$$

(Equation 3)

Total alkalinity (A_T) is a measure of the capacity of the water to neutralize hydrogen ions, balancing the electric charges in seawater. A_T is a quasi-conservative parameter, which can be influenced only by the massive proliferation of calcareous microalgae. The vertical variability of the chemical carbon pump is important because is one of the driving factors for the exchange of CO_2 seawater- atmosphere and drives CO_2 to the depth ocean (Legendre *et al*., 2015).

The magnitude of the ocean carbon sink depends on several competing effects in the CO_2 partial pressure differences across the air-sea interfaces due to differences in temperature. Seawater warming reduces solubility and increases pCO_2 in the mixed layer. When the seawater is colder, solubility in the water increase while when the temperature in the seawater is warmer, the solubility for the CO_2 in the water is reduced. The accumulation of CO_2 in the ocean decreases pH and shifts carbonate chemistry to high dissolved CO_2 gas fractions (Fung *et al*, 2005).

To determine the CO_2 difference between the surface waters and the atmosphere, it is necessary to evaluate the fugacity of CO_2 in seawater (fCO_2^{sw}) and in the atmosphere (fCO_2^{atm}). The fugacity of CO_2 is related to partial pressure, but it is not exactly the same since it is the product of the mole fraction (xCO_2^{atm}) times the total pressure. Fugacity takes into account the non-ideal nature of the gas phase (Dickson *et al*., 2007), rather than considering it as an ideal one. The difference between pCO_2 and fCO_2 can be usually assumed a 0.3%, a procedure sufficient accurate for the purpose of air-sea CO_2 (Lewis, 1998).

The interannual variations in the atmospheric forcing in response to modes of climatic variability and other physical and biological processes in the upper ocean, like upwelling, should play an important role in the determination of the interannual

variability of the CO_2 uptake in the global ocean (Borges and Frankignoulle, 2001; Olsen *et al.*, 2003).

1.4 BAKUN'S THEORY

Climate change is one of the most important challenges in our time. It is a change produced on a global scale but with effects in local terms and in different science fields. For example, in 2015 the average increase in temperature across global land and ocean surfaces was 0.9°C, and this was the highest among the overall 136 years of records from the Department of Commerce (2018) while the year before was only 0.16°C. One of the issues of this change will be the differences in the wind stress due to the differences in temperature caused by the greenhouse gasses accumulated in the atmosphere. So this challenge of climate change is changing the pattern of EBUS. The problem is to understand how global change is affecting these systems.

Within this approach, Bakun (1990) published a theory about this issue titled "Global Climate Change and Intensification of Coastal Ocean Up-Welling". This article was referring to an apparent paradox associated with the idea that global warming might lead to an intensified cooling of local areas affected by coastal upwelling (Barton *et al.*, 2013).

The theory is based on the substantial increase of CO_2 and other greenhouse gases in the atmosphere (IPCC, 2018), which will create an inhibition of cooling in the night that will develop a heating intensification in the continental zone adjacent to upwelling regions. For this author, the alongshore wind that drives coastal upwelling will be maintained in part by a strong atmospheric pressure gradient developed over the heated land mass and the higher barometric pressure over the cooler ocean (Bakun, 1990), rising wind stress that, will increase the intensity of the upwelling (Bakun and Weeks, 2004). For example, in the case of Iberian Peninsula, like in California, Bakun (1990) indicated an increase in the northeastern Atlantic Ocean wind stress during the spring to summer upwelling season between the 1950s and 1980s (Fig. 1.5). Nevertheless, the IPCC reports state that this "global warming" should not always lead an increase in the local temperatures.

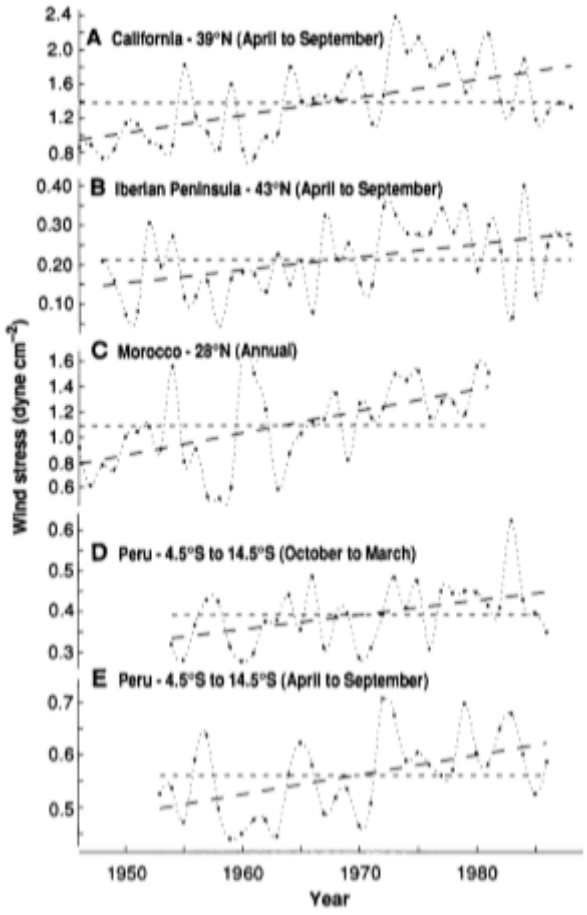

Figure 1.5: Year averages of monthly estimates of alongshore wind stress of California, Iberian Peninsula, Morocco, and Peru. Short dashes indicate the long-term mean of each series while longer dashes indicate the linear trend fitted by the method of least squares (Bakun, 1990).

In consequence, there are several scientists trying to test this theory in different locals of the planet. For example, data of significant cooling of surface waters from the coastal upwelling area off Cape Ghir (North West Africa near 30.5°N) during the latter part of the 20th century (Lemos and Pires, 2004) were reanalyzed by McGregor et al., (2007), and support the "Bakun hypothesis", while a decrease in coastal upwelling intensity of the coast of Portugal in the later part of the 20th century was observed (Narayan *et al*., 2010). As stated by Relvas *et al*., (2009) there is a time lag between the different projects and scales about how is changing the SST and Wind Stress, (microscale in the order of 10 m, mesoscale in the order of 50 km or macroscale in the order of >1000 km) that will conduct to a different conclusion regarding the increase or decrease of upwelling intensity. It is perceived by some scientists a warming-up trend in the Eastern North Atlantic and in the coastal regions (Relvas *et al*., 2009), which is in opposition to Bakun's hypothesis.

One variable that Bakun did not take into account was the North Atlantic Oscillation (NAO), which is an index based on the surface sea level pressure differences between the Subtropical Azores high cell and the subpolar low cell (Ncdc.noaa.gov, 2018). During a positive NAO, conditions are colder and drier than average over the northwestern Atlantic and Mediterranean regions, whereas conditions are warmer and wetter than average in Northern Europe, the Eastern of the United States and part of Scandinavia (Visbeck *et al*., 2001). NAO is widely recognized as the most significant pattern of climate variability in the North Atlantic sector (Visbeck *et al*., 2003) and it has shown modes that may lead simultaneously local warmer or cooler effects (Perez *et al*., 2010). It has been recognized too, that the fluctuations in SST and the strength of the NAO, are related, and there are clear indications that NAO varies significantly with the overlying atmosphere, and hence, it is possible that anthropogenic climate change might influence the natural variability of the NAO.

1.4.1 Bakun's theory application at the Rías Baixas

At the Rias Baixas on the Galician coast of Spain, despite the increase of winds for the Iberian Peninsula, there is a general weakening in upwelling intensity. There is an overall warming observed in the Iberian/Canary current region, that exceeds the mean oceanic values (Pardo *et al*., 2011), as reported by other authors, such as Sydeman et al., (2014) that reworked quantitatively data of wind trends information data from 22 studies published between 1990-2012. These data were used to test if the winds were increasing (consistent with Bakun's theory) or decreasing (inconsistent with Bakun's theory). The data provided and tested, support the hypothesis of wind intensification in the California and Humbolt systems, whereas the Iberian system was inconsistent with Bakun's hypothesis, by winds weakening. The authors concluded that the annual average wind trends did not support the upwelling intensification hypothesis (Sydeman *et al*., 2014). Relvas *et al*. (2009), using Sea Surface Temperature (SST) by satellite imagery, got a generalized warming trend in the coastal waters of the Western Iberian Peninsula for the period 1985-2003.

1.5 OBJECTIVES

Taking into account the Bakun theory application for the Rias Baixas, this thesis has as a major objective to estimate the annual CO_2 fluxes and upwelling in Galicia between 1997 and 2017. This work is important given the difficulty to monitor variables such as temperature, salinity, pH, in long-term scenarios provided by instrumentation, and the difficulty in taking measurements at sea (Casey and Cornillon, 2001).

To achieve this, specific objectives will be developed:

- To analyze the chemical changes associated with the large-scale variability of upwelling systems (CO_2 fluxes), physical variations in terms of upwelling and thermohaline, and biological forcings such as chlorophyll an (as a proxy of phytoplankton development) and net ecosystem production.

- Furthermore, it will be analyzed the long-term impact of CO_2 fluxes on primary production in the Galician coast.

2. VARIABLES TO CALCULATE AIR-SEA CO_2 FLUX AND UPWELLING INDEX

2.1 AIR-SEA CO_2 FLUX

There are many variables that can affect the calculations of the air-sea CO_2 flux (FCO_2) (Fig.2.1) The measurements of fugacity require normally, a gas phase balanced with sea water knowing pressure and temperature (Dickson *et al*., 2007). Nowadays, the major uncertainty in the calculation is attributed to the estimation of k (gas transfer velocity) parameter (Takahashi *et al*., 2009).

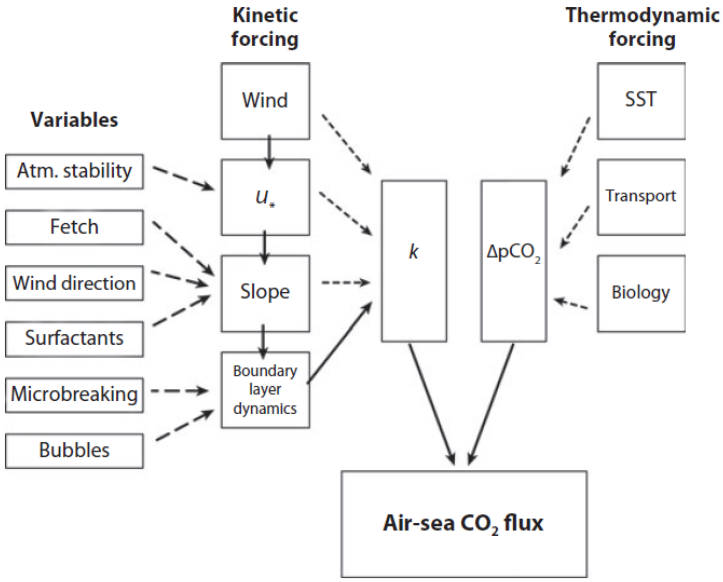

Figure 2.1: Variables that can affect the calculation of air-sea CO_2 flux, on the left, environmental forcing factors, on the right the factors that can affect the air-sea pCO_2 gradient (Wanninkhof et al., 2009).

This is parameterized as a function of the wind speed that is the main factor to relate to the gas transfer (Wanninkhof *et al*., 2009). The dependency differs a lot among studies, and it has been stated as linear, $k_{L\&M}$ (Liss and Merlivat, 1986) (Eq. 4), quadratic k_W, k_N, ks computed by Wanninkhof, 1992; Nightingale *et al*., 2000; Sweeney *et al*., 2007, respectively (Eq. 5, 6, 7), and cubic, $k_{M\&G}$, (McGillis *et al*., 2001; Eq. 8) where Sc refers to the Schmidt number and U_{10} refers to the wind speed; a, b and c are coefficients dependent on the wind speed and 600 and 660 are the Sc values in fresh water or sea water respectively, at 20ºC of temperature. Other physical processes affect the estimation of this constant, such as thermal stability, the presence of surface surfactants or rainfall. Due to the non-consensus with respect to the best k parameterization, it is

important to give special attention to the quality of the wind speed data, particularly using quadratic and cubic parameterizations. The sources can be different. The data taken from ships can be distorted due to the structure of the ship, which gives a bias in the data. It is possible to take the data from buoys too, but they are not totally consistent with the locations and time of the measurements of ΔpCO_2. Finally, model data and data from Satellites such as QuickSAT, Seawinds or SSM/I, are the best ones due to their homogeneity and quality in large spaces, with a high resolution (0.25º) (Otero *et al*., 2013; Remss.com, 2018)).

$$k_{L\&M} = (aU_{10} + b)\left(\frac{Sc}{600}\right)^{-c} \quad \text{(Equation 4)}$$

$$k_w = 0.31U_{10}^2\left(\frac{Sc}{660}\right)^{-0.5} \quad \text{(Equation 5)}$$

$$k_N = (0.222U_{10}^2 + 0.333U_{10})\left(\frac{Sc}{600}\right)^{-0.5} \quad \text{(Equation 6)}$$

$$k_S = 0.27U_{10}^2\left(\frac{Sc}{660}\right)^{-0.5} \quad \text{(Equation 7)}$$

$$k_{M\&G} = (3.3 + 0.026U_{10}^3)\left(\frac{Sc}{660}\right)^{-0.5} \quad \text{(Equation 8)}$$

xCO_2^{atm} seems not being a critical variable for the estimation of air-sea CO_2 fluxes. This is due to, the fact that in the high atmosphere the ratios in the mixing keep a seasonal variability of the CO_2 atmospheric molar fraction (xCO_2^{atm}) smaller than in sea-water (Padin *et al*., 2007).

The interest in gas fluxes in the ocean is related to a phenomenon happening at different temporal and spatial scales. To achieve the air-sea CO_2 flux, it is required to understand the influence of these factors (Fig.2.1) in the CO_2 flux. By convention, if a flux is negative means that the ocean is acting as a sink, while when the flux is positive, the ocean is acting as a source (Wanninkhof *et al*., 2009).

Upwelling phenomenon in coastal waters is an important process to take into account in the study of air-sea CO_2 flux. Upwelling brings to the surface, colder waters from the bottom, enriched in gasses like CO_2, both the changes in temperature an enrichment of CO_2 in surface waters provoke changes in the air-sea CO_2 flux.

2.2 UPWELLING INDEX DERIVED FROM BAKUN THEORY

The upwelling index used in this project is based on Ekman Transport and it is more appropriate for evaluating temporal variations of upwelling intensity (Lamont *et al*., 2017). Eq. 9 can be worth for purposes such as determining potential biophysical effects of anthropogenic global warming (García-Reyes *et al*., 2014).

$$I_w = -\left(\frac{\tau_y}{\rho_{sw} f}\right) = -\left(\frac{\rho_{air} C_D |V| V_y}{\rho_{sw} f}\right) \qquad \text{(Equation 9)}$$

Where ρ_{air} is the density of the air (1.22 kg m^{-3} at 15°C), ρ_{sw} is the density of the seawater (~ 1025 kg m^{-3}), f is the Coriolis parameter ($9.946 \cdot 10^{-5}$ s^{-1} at 43°N), τy is Shelf wind stress, C_D is an empirical dimensionless drag coefficient ($1.4 \cdot 10^{-3}$ according to Hidy, 1972), V and Vy are the average daily strength and a northerly component of the wind, respectively.

The upwelling index represents the offshore Ekman transport value but with a different sign. It will be positive when the Ekman transport is offshore and upwelling favorable (Herrera *et al*., 2005).

There is a possibility SST-based index which provides a good representation of the spatial variation of upwelling (Lamont *et al*., 2017). Nevertheless, the one derived by Bakun, (1973) (Eq. 9) was the one chosen for this project and it has been chosen for decades. The formula is an estimation of the cross-shelf Ekman transport due to geostrophic wind stress calculated from large-scale atmospheric pressure gradients (García-Reyes *et al*., 2014).

To measure the upwelling index there are another ways, for example in coastal zones upwelling is driven by a cyclonic curl of wind stress, this cyclonic curl is one order of magnitude lower than Ekman transport (Lamont *et al*., 2017).

3. MATERIAL AND METHODS

3.1 STUDY AREA

The study area where pCO_2 data were taken corresponds to a large coastal embayment close to Vigo (Gago *et al*., 2003) as shown in Fig. 3.1. These data derived from several oceanographic cruises made by the Marine Research Institute belonging to the Spanish National Research Council (IIM-CSIC) in Vigo (Spain). The final database used to cover the area from 42°N to 43°N and from coast to 10.5°W, the longitude that marks the eastern boundary of the Iberian Current (Alvarez *et al*., 2009). The ria was divided into Inner, Middle and Outer zones following the same pattern as described by Gago *et al*., (2003).

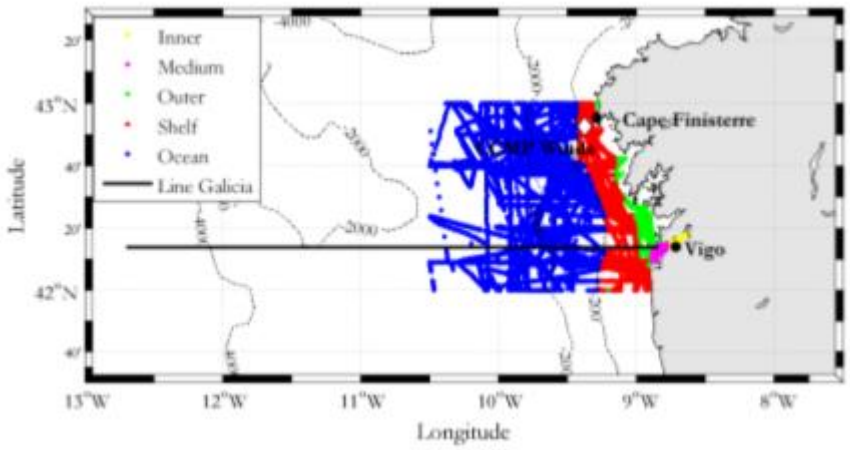

Figure 3.1: Map of the Galician rías, continental shelf, and ocean, showing the five studied zones: "Inner" (data from 8.64ºW to 8.78ºW, yellow) and "Middle" (8.78ºW to 8.9ºW, magenta); "Outer" for the data measured outside the Ría de Vigo from 8.9ºW until 50 m depth (green); "Shelf" for the data measured between 50-200 m depth (red); and "Ocean" for data measured from 200 m depths until 10.5ºW (blue).

3.2 OCEANOGRAPHIC CRUISES

Working data were taken from different oceanographic cruises embedded in different projects such as, Dynamics and Biogeochemical short-scale variability in the Galician continental shelf – DYBAGA; Evolution of CO_2 increase using ships of Opportunity: Galicia and Bay of Biscay – ECO; CUBE; Community Structure, Trophic Functioning, and Biogeochemical Plankton Rates during downwelling in the Coastal Transition Zone

of NW Spain – ZOTRACOS; and Reactivity of Dissolved Organic Matter in the upwelling system of the Ría de Vigo – REMODA, NAVAZ and finally the one that is actually running ARIOS (Acidificación en las Rías y Plataforma oceánica ibérica). The data that were not possible to take from these oceanographic cruises, were taken from SOCAT which are data from other Oceanographic campaigns of other National Research Institutes.

ARIOS project is explained in detail since there was a personal participation on it to learn each step. The data were processed from the beginning with raw data for 2017 and 2018, while the rest of the data were in another state of processing or downloaded from a database.

For ARIOS project, samples were taken in 9 stations along the transect (Fig.3.2, Table 1.1). The stations in the outer part of the Ria were 1, 2, 3, 4 and 5 while inside were 6, 7, 8 and 9. In each station was thrown a rosette with 12 Niskin bottles (Fig.3.3). The samples were taken thinking in the exchange of gases, being the oxygen the first one to be sampled, using a thermometer to determine a constant temperature using the Winkler method (Winkler, 1888). Secondly, the cuvettes for pH were sampled. Next, it was taken samples for determination of alkalinity, nutrients, and salinity. For all the samples it was important to take the samples without bubbles. Finally, it was taken the samples for chlorophyll, with a volume of 250 mL using a test tube which was filtered in the ship and the filters were kept in a freezer in tubes wrapped in aluminum foil to avoid to degradation of the chlorophyll until further analysis in the laboratory.

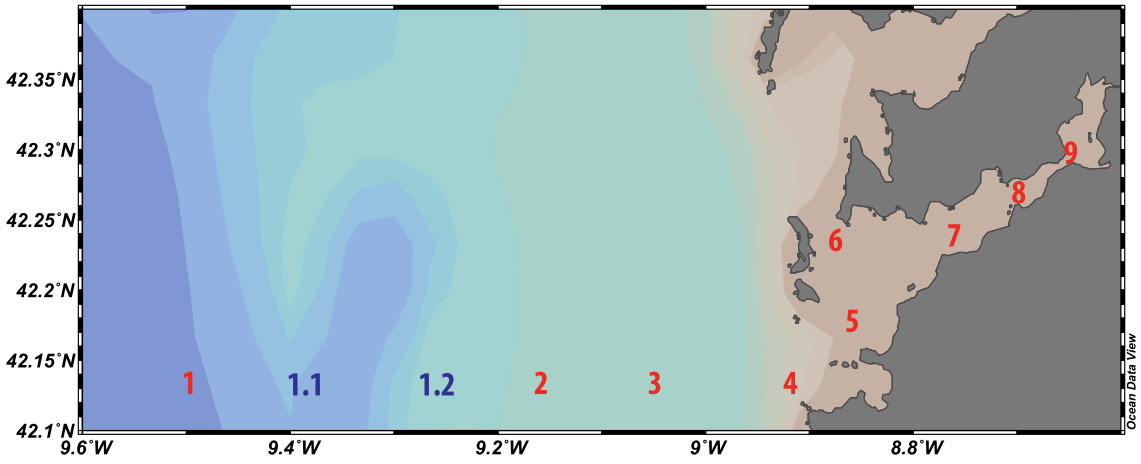

Figure 3.2: Stations along the coastal zone and ocean interior where samples are taken in ARIOS campaigns.

Table 1.1

ST in the show the locations from the map. The number of levels where there were taken samples, Zmax, is the maximum depth where there were taken samples.

ST	*Lat (ºN)*	*Lon (ºW)*	*Nº Levels*	*Z MAX*
1	*42º 7.980'*	*9º 30.000'*	*11*	*200*
1.1	*42º 7.980'*	*9º23.352'*	*CTD*	*200*
1.2	*42º 7.980'*	*9º16.686'*	*CTD*	*200*
2	*42º 7.980'*	*9º 10.020*	*10*	*150*
3	*42º 7.980'*	*9º 3.000'*	*9*	*125*
4	*42º 7.980'*	*8º 56.760'*	*7*	*80*
5	*42º 9.720'*	*8º 53.520'*	*6*	*50*
6	*42º 14.820'*	*8º 53.100'*	*4*	*22*
7	*42º 14.400'*	*8º 45.720'*	*5*	*40*
8	*42º 16.200'*	*8º 42.120'*	*5*	*22*
9	*42º 17.520'*	*8º 39.120'*	*3*	*20*

Figure 3.3: Rosette with 12 Niskin Bottles.

In order to improve the characterization of the section, there were done two stations 1.1 and 1.2 (Fig. 3.2), in which, it was thrown a CTD and a Fluorometer Turner. Inside the ship, there were continuously measurements along the whole campaign of dissolved oxygen with an Optode (Aanderaa), of pH with an AFT Sunburst and chlorophyll *a* with a fluorometer (SeaFet). The pH measurements were afterward used to calculate the pCO_2 in water.

3.3 DATA TREATMENT

3.3.1 Laboratory measurements

Salinity samples were collected in all stations at selected depths to calibrate the conductivity sensor installed in the CTD bathysonde and in the underway thermosalinograph. Samples were stored for 24 hours in the laboratory under controlled temperature (22ºC) before analysis (Fig. 3.4a). During the first leg of the cruise, salinity samples were collected in all stations at 3 selected depths (two in deep water and one in the surface) and were analyzed using PORTASAL Guideline and calibrated with one only existing IAPSO standard seawater. A container of 50 liters was filled with seawater collected at 2500 meters depth at station 5. This water was used during the cruise as a substandard during the cruise and was analyzed at the beginning and at the end of each series of analysis to check the drift of the PORTASAL.

During the same day of the cruises, it was important to start the measurements of seawater pH samples which were taken at 24 levels in all the stations along the FICARAM-XVII section. pH measurements were made using the spectrophotometric method described in Clayton and Byrne, (1993). This method consists of adding 75 µL of m-cresol purple (mCP) to the seawater sample and measuring its absorbance at 3 wavelengths, i.e., λ_{HI}=434 nm; λ_{I}=578 nm and $\lambda_{non\text{-}abs}$=730 nm (Fig. 3.4b). The reaction of interest at seawater pH is the second dissociation (Eq. 10) in which I is the indicator. Then, the total hydrogen ion concentration can be determined by Eq. 11. pH samples were taken directly from the Niskin bottles into special optical glass spectrophotometric cells of 28 mL of volume and 100 mm of path length. These cells were carefully stored in a thermostatic bath at 25.0ºC around one hour before the analysis. Absorbance measurements were performed with a Perkin Elmer Lambda 850 UV-VIS spectrophotometer on board the R/V Hespérides. pH values were given following the

equations described in Dickson *et al*. 2007, who includes a correction due to the difference between seawater and the acidity indicator (ΔR).

$$HI^{-}_{(aq)} = H^{+}_{(aq)} + I^{2-}_{(aq)} \qquad \text{(Equation 10)}$$

$$pH = pK_2 + \log_{10}[I^{2-}]/[HI^{-}] \qquad \text{(Equation 11)}$$

After this, during the next day, it was measured the samples of A_T which were taken during the FICARAM section every each station, almost half of the total stations. In order to analyze these A_T samples on board, the water was transferred directly from the Niskin bottle to 600 mL borosilicate glass bottles and stored for 24 hours before the analyses. Measurements of A_T were done by a one endpoint method using an automatic potentiometric titrator (Dosino 800 Metrohm) with a combined glass electrode (Fig. 3.4c). A Knudsen pipette (~195 mL) was used to transfer the samples into an open Erlenmeyer flask in which the potentiometric titration was carried out with HCl (0.1 M). The final volume of titration was determined by means of one pH endpoint (Körtzinger *et al*., 1996). In order to estimate the accuracy of the A_T method, A_T measurements of certified reference material (CRM) for CO_2 from batch 100 provided by Dr. Andrew Dickson was analyzed. In addition, an extra calibration (substandard) was made by using a closed container of 75 L filled with open ocean surface water.

Figure 3.4: (a) the salinometer, (b) spectrophotometer to measure pH, (c) titration apparatus to measure alkalinity.

For this project, pH was measured continuously as well as other parameters such as sea surface temperature (SST), sea surface salinity (SSS) which gave the data to calculate alkalinity, to determine pCO_2^{sw}. However, it was important to take samples and analyze them in the laboratory. Using this procedure it was possible to correct the measurement done in continuous. Measurements done in the laboratory are more reliable than the ones taken with a sensor.

3.4 ESTIMATION OF CO_2 AIR-SEA EXCHANGE

3.4.1 Data script preparation: fCO_2^{sw} calculations

First of all, it was necessary to determine the Alkalinity. With alkalinity data from the laboratory, it was determined a regression line with data of a whole year for the surface values of both SSS and Alkalinity. With these linear equations, it was determined the alkalinity from the continuous data of SSS (Eq. 12). Eq. 12 is an example for the years 2017 and 2018 for the ARIOS project, where y=Alkalinity and x=SSS.

$$y = 57.442 * x + 295.62 \qquad \text{Equation 12}$$

$$R^2 = 0.80$$

With pH, it was done the same procedure using the data measured in the laboratory and making the linear equations with the data registered with the AFT Sunburst for each campaign, matching the data where there were values of both measurements. Then pH was corrected using again the linear equation. After these calculations, for the pH corrected it was done a running mean to determine an average value of the data using MATLAB software as we can see in the example in Fig. 3.5.

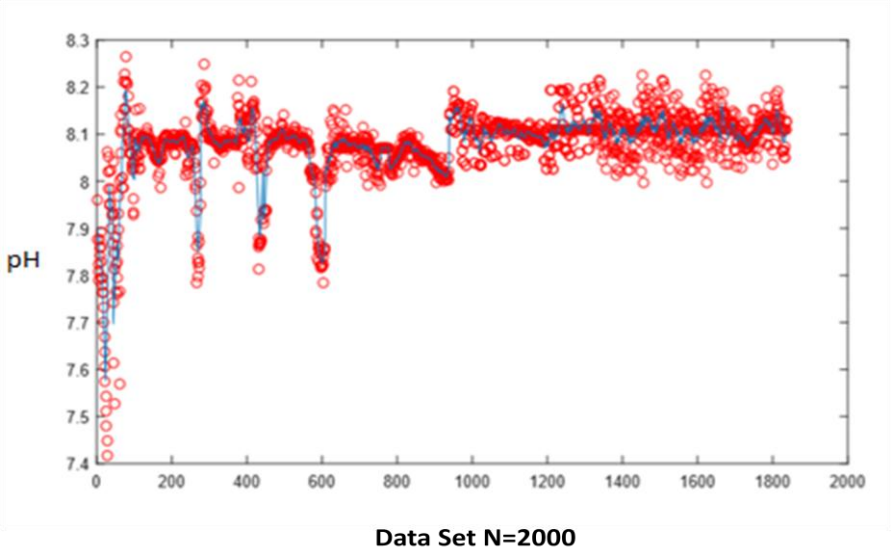

Figure 3.5: Running mean in blue and raw data in red, from the pH data corrected, this data are from 2017 and 2018.

Knowing both pH and Alkalinity it was possible to calculate pCO_2^{sw}. This calculation was done from the campaigns explained before, between 1997 and 2018, to better understand the long-term variability since there were some gaps in the data set. When there were not campaigns data were attained from SOCAT where data from other Oceanographic campaigns of other National Institutes Research exist. The transformation of pCO_2 into fCO_2 was done through the difference between them which is lower than 0.3% (Weiss, 1974; Olsen *et al.*, 2003).

3.4.2 Data script preparation: fCO_2^{atm} calculations

The data of atmospheric CO_2 fugacity was estimated from the monthly values of atmospheric CO_2 molar fraction recorded in meteorological stations of the NOAA/ESRL Global Monitoring Division stations, Mace Head (mhd) and Izaña (Izo) (Fig. 3.6). The xCO_2^{atm} were linearly interpolated versus latitude for the calculations of CO_2^{atm}, while the final xCO_2^{atm} dataset was converted to atmospheric CO_2 partial pressure (pCO_2^{atm}) (Eq. 13). With this aim, first, to calculate the water vapor pressure (pH_2O) it was used the formula from Weiss and Price (1980), where S and T were salinity and temperature (ºC) (Eq. 14). The final xCO_2^{atm} dataset was converted to pCO_2^{atm}, considering P_{atm} and pH_2O (in atm), which was calculated from in situ SST readings (Eq. 13) (Weiss, 1974). The pCO_2 values were then converted to fCO_2^{atm} assuming a decrease of 0.3% from the pCO_2^{atm} value (Weiss,1974), due to the non-ideal behavior of carbon dioxide (Gago *et al*., 2003).

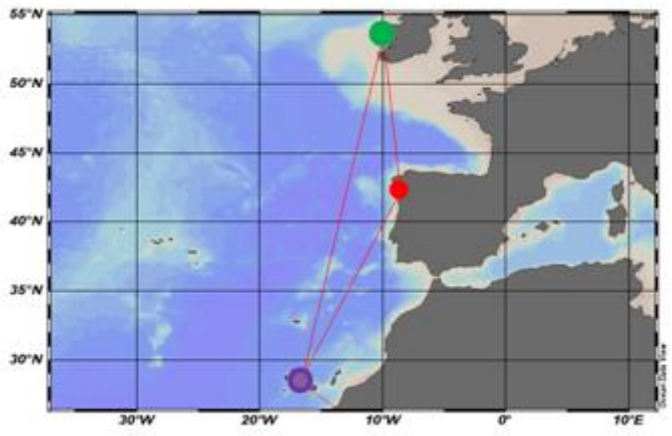

Figure 3.6: Izaña is the purple point situated in the Canary Islands, Mace Head is the green point situated in Irland both forming a triangle with the zone of this project in Galicia, redpoint.

The more recent data out of a period that covers the data series for both stations between 2010 and 2017, were estimated extending the seasonal variation from the interannual tendency observed from 2010 to 2017, until 2018.

To calculate the water vapor pressure (pH_2O) that enters in the calculation of the pCO_2^{atm} it was used the formula from Weiss and Price (1980), where S and T were salinity and temperature (ºC) (Eq. 14). The final xCO_2^{atm} dataset was converted to

pCO_2^{atm}, considering P_{atm} and pH_2O (in atm), which was calculated from in situ SST readings (Eq. 14) (Weiss, 1974).

$$pCO_2^{atm} = xCO_2^{atm} (P_{atm} - pH_2O) \qquad \text{(Equation 13)}$$

$$pH_2O\ (S,T) = \exp\left(24.4543 - 67.4509\left(\frac{100}{T}\right) - 4.8489 \ln\left(\frac{T}{100}\right) - 0.000544S\right)$$

(Equation 14)

3.4.3 Data script preparation: FCO_2 Flux calculations

The CO_2 exchange between the ocean and the atmosphere (FCO_2, in mol m^{-2} yr^{-1}) was calculated by Eq. 15, where K was the CO_2 gas transfer velocity (cm h^{-1}, estimated from wind speed), S was the solubility of the CO_2 in the seawater estimated according to Weiss, 1974 and ΔpCO_2 was the difference between pCO_2^{sw} and pCO_2^{atm}. A negative flux means that the ocean was absorbing atmospheric CO_2 while a positive flux means that the ocean was emitting CO_2 into the atmosphere.

$$F = k \times S \times \Delta pCO_2 \qquad \text{(Equation 15)}$$

K parameter, as it was explained before, is a crucial parameter that depends mainly on the quality of the wind speed data that was calculated using the Cross-Calibrated Multi-Platform (CCMP) (Remote Sensing Systems, 2018) which is a remote sensing system.

3.4.4 Complementary data sources

3.4.4.1 NEP data

Net Ecosystem Production (NEP) was included in the dataset as a proxy for photosynthetic activity (Science.oregonstate.edu, 2018). It was obtained by the Vertically Generalized Production Model (VGPM) (Behrenfeld and Falkowski 1997) that is fed by Chl *a*, SST, and photosynthetically active radiation (PAR) information as inputs, which was obtained from Sea-viewing Wide Field of view Sensor (SeaWiFS) and Moderate Resolution Imaging Spectroradiometer (MODIS) Sensor. It was downloaded and interpolated using "nearest-neighbor" since the data was taken from a transversal line which included all zones, from -8.64ºW to -13ºW in the latitude 42.2ºN. Afterward, it was calculated the average for each month.

3.4.4.2 Wind speed, chlorophyll, and NAO data source

In order to make the calculations of upwelling index (Eq. 9), it was used data of Wind speed and SST which was obtained from (NCEP/NCAR Reanalysis I). In this case, it was decided to use this SST data and not the continuous data because of the scale of upwelling is much bigger and the continuous data measured in-situ could give larger errors while drawing conclusions.

Chlorophyll was taken from, SeaWiFS between 1997 and 2010 with a 9 km resolution, and from MODIS between 2011 and 2018 with a 4 km resolution (Oceandata.sci.gsfc.nasa.gov, 2018). These data of Chl*a,* were important to make the correlation with the NAO index. Finally, monthly data of NAO Index was taken from "Climate Prediction Center - Teleconnections: North Atlantic Oscillation", (2018).

3.5 BIOCHEMICAL FORCINGS

3.5.1 fCO_2^{sw} variability between biological and temperature components

For both Eq. 16 and 17 SST_{mean} is the annual average in ºC, and SST is sea surface temperature observed in ºC. fCO_2^{sw} is the data observed in atm (Eq.16) while $fCO_2^{sw}{}_{mean}$ is the annual average of the fCO_2^{sw} observed (Eq. 17). Both formulas were used to explore how much the final fCO_2^{sw} data (Takahashi *et al*., 2002) is affecting the thermodynamic component and the biological component.

$$^{B}fCO_2^{sw} = fCO_2^{sw} \exp\left[0.0423(SST_{mean} - SST)\right] \qquad \text{(Equation 16)}$$

$$^{T}fCO_2^{sw} = fCO_2^{sw}{}_{mean} \exp\left[0.0423(SST - SST_{mean})\right] \qquad \text{(Equation 17)}$$

3.5.2 Seasonality of the variables

Eq. 18 was done to model the variability of the fCO_2 considering its drivers: SST, SSS, and Chl*a*). Simultaneously, it includes the seasonal cycle to model the temporal variation, being the seasonal cycle of major importance than its drivers. For the seasonal cyclicity, it was used 4 harmonics with a period of 12, 6, 4, and 3 months.

The SST had a special treatment, by calculating the SST anomalies, which were the values above or below the average SST in each moment. When SST anomalies were positive, the saturation of fCO_2^{sw} increases as it was expected, and when SST anomalies

were negative, these should diminish the saturation of fCO_2^{sw}. However this does not happen because when there is a negative SST anomaly, that can be upwelling, the waters are rich in dissolved gases as CO_2. For this reason, it is important to test both SST anomalies split in SST>0 and SST<0.

$$fCO_2^{sw} = fCO_2 + \sum_{i=1}^{4} b_i \times \sin\left(\frac{2\pi(t-\varphi)}{365.25}\right) + tfCO_2 + A \times (SST > 0) + B \times (SST < 0) + C \times SSS + E \times Chl\ a \quad (18)$$

3.5.3 Statistical Analysis

The normality of the different variables was checked by using Software SPSS with a test of Kolmogorov-Smirnov. It was added two new variables apart from SST, SSS, Chla, ΔfCO_2, FCO_2 and I_w, which were NAO Index taken from Department of Commerce-NOAA, (2018) and Winter NAO Index which was a group of data done when the differences of the NAO Index are higher as during December, January, and February. Using monthly averaged for all the variables, the data was split into two groups, Ria and Off-shore. Because the Kolmogorov-Smirnov test was normal, it was elected a Pearson correlation to determine the relationship between variables. This was done with the aim of observing if there is some relationship between the studied variables between 1997 and 2018 and the NAO.

4. PRECEDING RESULTS

Figure 4.1 shows the data since 2010 of levels of xCO_2 in the atmosphere. This was an important parameter to determine the CO_2 flux difference between seawater and atmosphere. There is a tendency to increase each year, having seasonal variation in the same proportion every year. This was one of the important parameters to support Bakun's theory of Wind Stress diminishing.

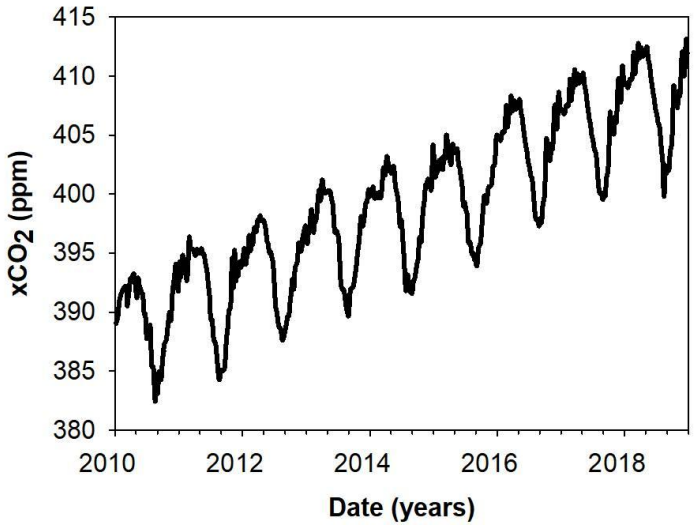

Figure 4.1: Data downloaded from xCO_2, 2018 is an estimation from the past years.

Figure 4.2 has two important variables to calculate fCO_2^{sw}, Fig.4.2a is the pH that remains constant during 2017 and 2018. Alkalinity has the same constant behavior which is important when determining fCO_2^{sw}. Alkalinity (Fig.4.2b) acts as a tampon which is the capacity to maintain a stable pH along time. Both together can allow the calculation of pCO_2 contained in the sea-water at a certain time.

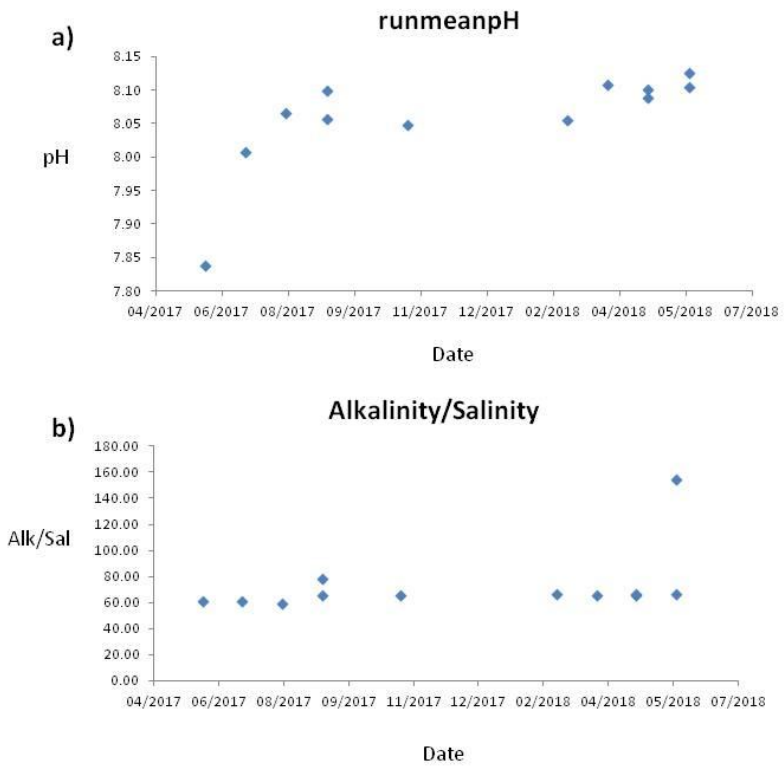

Figure 4.2: (a) Daily average of pH taken over the cruises in continuous, between 2017 and 2018 embedded in the ARIOS project. (b) data of specific alkalinity calculated from SSS data taken in continuous embedded in ARIOS project.

5. RESULTS

5.1 DATA AVAILABLE FOR THIS PROJECT

As it is possible to observe in Fig. 5.1, there are years with no data available, and that there is not the same amount of data for the different zones, which is important and an issue to have in account when discussing the results and drawing conclusions. The Ría de Vigo, represented by the Inner, Middle and Outer zones, have less data, in opposition to off-shore represented by Shelf and Ocean. There is a gap of data between 2006 and 2008 for the overall zones. The colors presented for the different zones will be the same ones for the rest of the project.

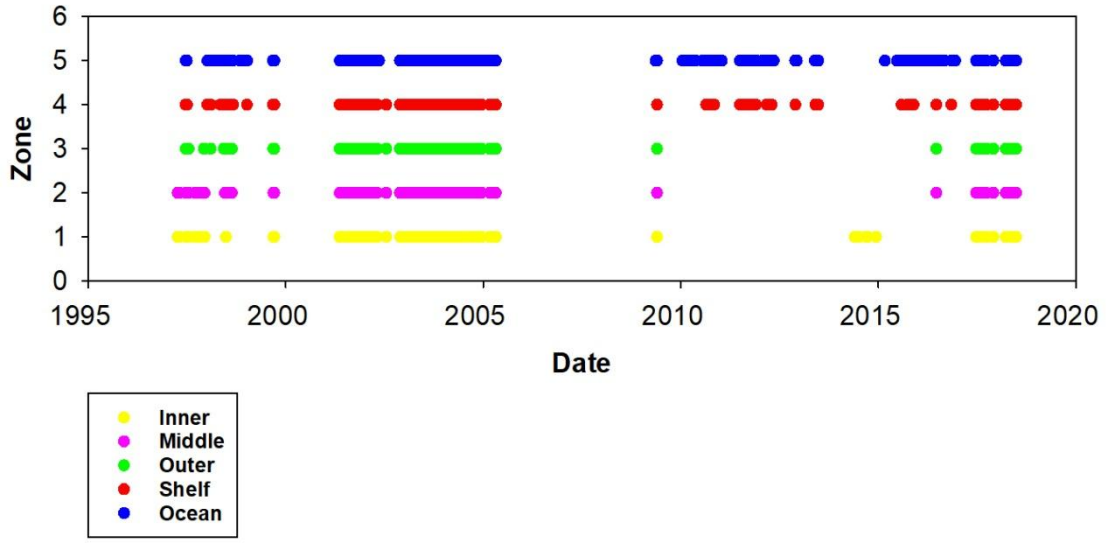

Figure 5.1: Data available for this project for the different zones.

5.2 SEASONAL VARIABILITY

5.2.1 Seasonal variability of SST, SSS, FCO_2, ΔfCO_2, and NEP

As can be observed in Figs.5.2 and 5.3, SST maintained consistently the seasonal variability in the 5 zones, with higher values in summer and lower during winter, as expected. During the summer it is observed a decrease of temperature in August for all the zones, less pronounced in the middle zone. In all the cases, the maximum values of SST coincided both before and after the peak of the upwelling period. During Summer, when the solar radiation is higher it was achieved a maximum SST for the whole area in

the Ocean zone of 20.2 ºC on September (18.8±1.4 ºC, Table 5.1) when the occurrence of upwelling is decreasing (Fig. 5.4).

Minimum SST in all over the area are achieved during winter season, but there is a clear difference between the Inner and Middle zones, in January (12.2 ºC and 12.1 ºC respectively, Table 5.1), and the Outer, Shelf, and Ocean zones (12.6 ºC, 12.9 ºC, and 13.1 ºC respectively, Table 5.1), in March.

The highest differences in a month (referring to the SD) of SST was found during Summer when there is the major upwelling prevalence (Fig. 5.4). Upwelling brings colder waters from the bottom to the sea surface waters and changes drastically the temperature during this season. The lowest monthly SD between SST was recorded during the Winter months when there is downwelling.

In the case of SSS, this variable is relatively homogeneous in the Ocean with a maximum SD of 0.24 during July (Table 5.1). The Outer and Shelf zones behave like transition zones where the maximum SDs were recorded during the winter season, 0.95 and 1.13, in March and January respectively (Table 5.1). In the case of Inner and Middle zones, since these zones are the nearest to the continental run-off of fresh water, the variability of salinity is maximum, with the highest SD of 3.69 and 1.51 found in December and January respectively (Table 5.1). In the case of the Inner zone, salinity decreased to values lower than 30 during December (Table 5.1 and Fig. 5.2).

ΔfCO_2, which is the difference between fCO_2^{sw} and fCO_2^{atm}, is the capacity of absorbing more or less fCO_2 by the sea water. If the value is negative, then there is the capacity to absorb more but if it is positive then, the seawater cannot absorb more CO_2. Because the fCO_2^{sw} depends on many variables such as SST, the SD of ΔfCO_2 in each moment can change rapidly. This is the reason why the SD has a higher range in Table 5.1 than SST and SSS variables (Table 5.1).

The maximum values of ΔfCO_2 inside the Ria correspond to October (Figs. 5.2 and 5.3). The Inner zone is where the maximum positive value of 194 µatm was achieved, showing an inverse behavior with respect to salinity. In the Off-shore the values are much less positive with a maximum of 2 µatm in the Shelf (Table 5.1) and -1 µatm in the Ocean (Table 5.1), both in November and September respectively. The minimum values were achieved inside the Ria during May in the Inner and Outer zones (Fig. 5.2)

with values of -94 µatm and -96 µatm respectively (Table 5.1). The minimum value was achieved in the Middle zone in June (Fig. 5.2) with -74 µatm (Table 5.1). In the Off-shore, the Shelf and Ocean both achieved their minimum values of -78 µatm during May (Table 5.1 and Fig. 5.3). The highest SD was achieved in the Inner zone in August when the upwelling achieves his maximum with an SD value of 119 µatm (Table 5.1), followed by the Outer, Middle, Shelf, and Ocean, being the SD more homogeneous.

FCO_2 is related with ΔfCO_2, along with other two variables which are the CO_2 gas transfer velocity and the estimated solubility of the CO_2 in the seawater, giving a more precise information if the seawater is acting as a source or a sink of CO_2. FCO_2 values shown Figs. 5.2 and 5.3, it is possible to observe that sea water acts as a sink from April to June achieving the maximum sink value during May, while seawater act as a source from July to September. The Inner zone achieved the maximum value of 179 $mmolCm^{-2}d^{-1}$ in August (Table 5.1), matching the highest values of ΔfCO_2. The second maximum value in the Inner zone was 191 µatm (Table 5.1) in August, coinciding with the maximum upwelling index too (Fig. 5.4). The Inner zone is also where there was the minimum value, i.e. where the seawater act as a sink strongly (Fig. 5.2). In the Off-shore, most of the time, seawater acts as a sink of CO_2 (Fig. 5.3).

NEP was obtained from remote sensing and interpolated using data from the database. There is no data for NEP in the inner zone but there is a higher increase in the middle zone achieving its maximum of 8065 $mgCm^{-2}d^{-1}$ in August (Table 5.1 and Fig. 5.2), while the ocean zone is much less productive, achieving the minimum of 835$mgCm^{-2}d^{-1}$ in January (Table 5.1 and Fig 5.3). It also depicts a similar behavior as ΔfCO_2, showing an increase in the NEP when the fCO_2^{sw} is positive, releasing CO_2 into the atmosphere, despite that is not so obvious in Fig. 5.2 due to the scale of FCO_2. It is possible to see a relationship of the release of CO_2 to the atmosphere and the increase in the NEP, particularly inside the Ria where there is much more NEP. After the peak, around September there was an increase in the release of CO_2 to the atmosphere found the Middle zone. In the Off-shore case it is also possible to observe the same pattern around September, but despite the increase of the fCO_2^{sw} it is not enough to be a source of CO_2 to the atmosphere.

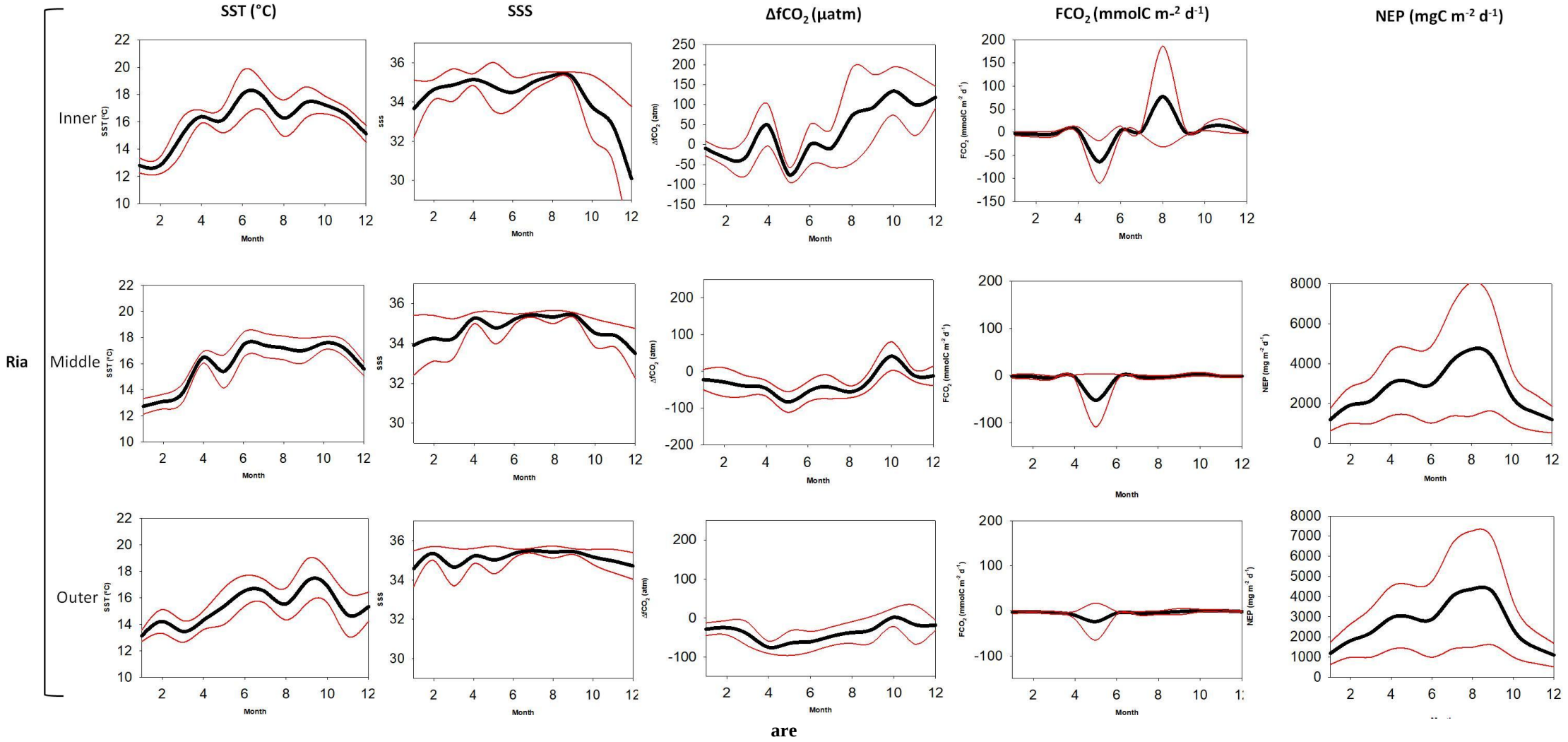

Figure 5.2: Monthly variability of the Ria de Vigo (Inner, Middle and Outer zones), of SST (°C), SSS, ΔfCO_2 (µatm), FCO_2 (mmolC m^{-2} d^{-1}), NEP (mgC m^{-2} d^{-1}) between 1997 to 2018. Red Lines the SD or typical deviation and the black line represent the average values.

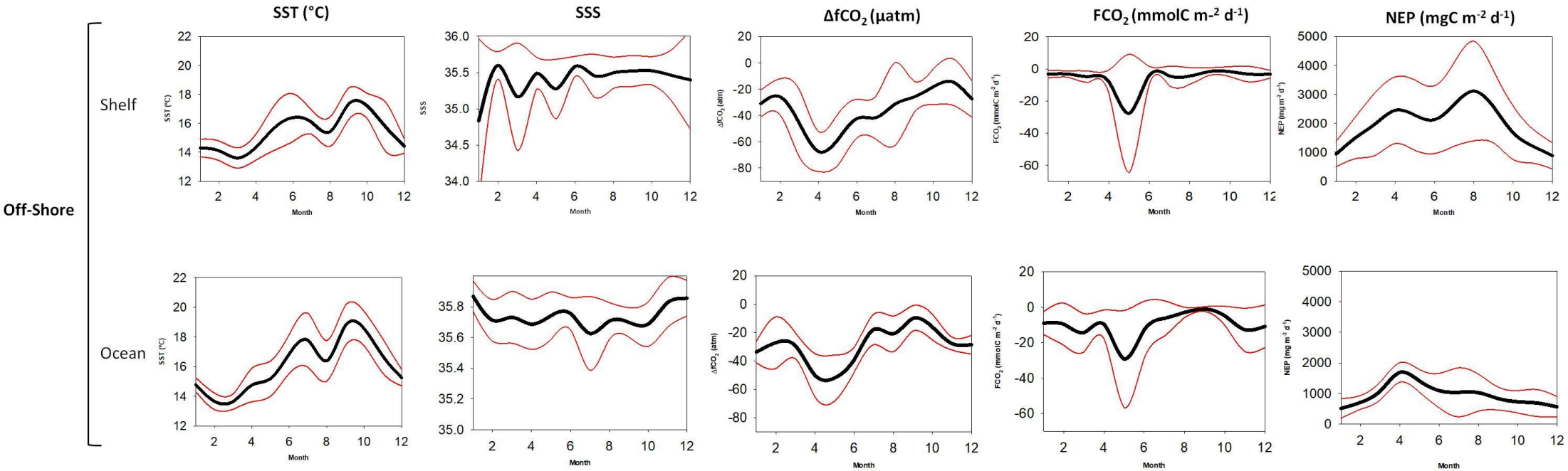

Figure 5.3: Monthly variability from the Shelf and Ocean of SST (°C), SSS, ΔfCO_2 (µatm), FCO_2 (mmolC m^{-2} d^{-1}), NEP (mgC m^{-2} d^{-1}) between 1997 to 2018. Red Lines are the SD or typical deviation and the black line represent the average values.

Table 5.1

Show data from Inner, Middle, Outer, Shelf, and Ocean zones, of SST (°C), SSS, ΔfCO_2 (atm), FCO_2 (mmolC m^{-2} d^{-1}), NEP (mgC m^{-2} d^{-1}), excepting the Inner zone where there is no data fot NEP.

Inner

Month	SST ± SD	SSS ± SD	ΔfCO_2 ± SD	FCO_2 ± SD
1	12.8±0.5	33.67±1.45	-9±18	-3±4
2	12.8±0.6	34.64±0.51	-33±23	-4±6
3	14.9±1.3	34.87±0.83	-27±49	-2±5
4	16.4±0.5	35.15±0.30	49±52	3±8
5	16.1±0.9	34.81±1.22	-76±18	-64±46
6	18.0±1.7	34.50±0.80	0±50	3±10
7	17.8±1.0	35.01±0.41	-10±47	2±7
8	16.3±1.3	35.34±0.20	72±119	78±109
9	17.4±1.2	35.29±0.25	92±83	4±13
10	17.2±0.7	33.76±1.61	134±60	10±7
11	16.6±0.5	32.91±1.77	100±78	13±14
12	15.1±0.6	30.09±3.69	118±27	-0±3

Middle

Month	SST ± SD	SSS ± SD	ΔfCO_2 ± SD	FCO_2 ± SD	NEP ± SD
1	12.7±0.6	33.91±1.51	-22±28	-2±4	1184±561
2	13.1±0.6	34.26±1.14	-29±39	-2±5	1918±912
3	13.8±0.7	34.27±0.98	-40.0±29	-4±3	2130±1148
4	16.5±0.4	35.28±0.28	-47±21	-3±4	3011±1634
5	15.4±1.3	34.79±0.80	-83±28	-53±56	3063±1684
6	17.5±1.0	35.22±0.27	-56±28	-5±7	2939±1926
7	17.4±0.9	35.44±0.13	-42±32	-2±4	4094±2729
8	17.2±0.9	35.34±0.33	-56±16	-4±3	4714±3351
9	17.0±1.0	35.42±0.12	-21±26	-1±3	4385±2759
10	17.6±0.5	34.53±0.70	41±39	3±4	2372±1349
11	17.2±0.6	34.41±0.59	-8±16	-1±2	1605±947
12	15.6±0.5	33.51±1.25	-12±27	-1±3	1188±671

Outer

Month	SST ± SD	SSS ± SD	ΔfCO_2 ± SD	FCO_2 ± SD	NEP ± SD
1	13.1±0.4	34.57±0.90	-29±16	-3±3	1180±553
2	14.2±0.9	35.34±0.35	-25±18	-2±2	1818±829
3	13.4±0.8	34.64±0.95	-42±30	-4±3	2209±1216
4	14.3±0.7	35.21±0.38	-75±16	-10±8	2947±1562
5	15.4±1.4	35.01±0.70	-65±31	-24±41	2959±1607
6	16.5±1.1	35.33±0.24	-61±26	-4±3	2875±1886
7	16.4±0.9	35.48±0.13	-47±24	-5±4	4015±2618
8	15.5±1.2	35.41±0.30	-37±28	-4±4	4376±2889
9	17.2±1.7	35.44±0.14	-29±34	-2±7	4226±2626
10	16.9±1.3	35.16±0.38	2±24	0±3	2374±1376
11	14.7±1.6	34.96±0.58	-17.±50	0±2	1514±817
12	15.3±1.1	34.71±0.67	-18±13	-2±2	1095±582

Shelf

Month	SST ± SD	SSS ± SD	ΔfCO_2 ± SD	FCO_2 ± SD	NEP ± SD
1	14.3±0.6	34.83±1.13	-31±10	-3±2	943±442
2	14.1±0.7	35.60±0.19	-26±14	-3±2	1518±732
3	13.6±0.7	35.16±0.74	-46±26	-5±3	1995±1094
4	14.4±0.9	35.49±0.22	-67±15	-8±7	2457±1152
5	15.7±1.6	35.27±0.41	-59±19	-28±37	2288±1217
6	16.4±1.6	35.58±0.14	-42±15	-4±6	2134±1173
7	16.1±0.8	35.46±0.29	-42±16	-4±6	2656±1445
8	15.4±1.0	35.50±0.21	-31±31	-4±5	3121±1726
9	17.4±1.1	35.52±0.21	-26±12	-2±2	2585±1254
10	17.2±0.9	35.52±0.19	-18±14	-2±3	1686±930
11	15.8±1.7	35.46±0.35	-14±18	-3±5	1218±591
12	14.4±0.5	35.40±0.68	-27±14	-3±2	881±453

Ocean

Month	SST ± SD	SSS ± SD	ΔfCO_2 ± SD	FCO_2 ± SD	NEP ± SD
1	14.8±0.5	35.87±0.10	-34±7	-9±6	514±321
2	13.7±0.6	35.71±0.13	-27±18	-9±12	714±228
3	13.6±0.5	35.73±0.17	-29±9	-14±11	1084±292
4	14.8±1.1	35.69±0.16	-50±15	-9±8	1692±320
5	15.2±1.2	35.74±0.15	-52±16	-29±27	1412±371
6	16.9±1.3	35.76±0.10	-39±9	-13±16	1098±565
7	17.8±1.8	35.63±0.24	-18±11	-6±10	1039±800
8	16.4±1.4	35.71±0.12	-21±12	-3±3	1028±604
9	18.8±1.4	35.70±0.10	-10±9	-1±1	837±378
10	18.6±1.2	35.69±0.14	-16±9	-5±5	731±364
11	16.7±1.2	35.83±0.16	-28±4	-13±12	689±441
12	15.3±0.6	35.85±0.11	-29±6	-11±12	566±338

5.2.2 Seasonal variability of Upwelling Index – derived from Bakun Theory

The upwelling index is presented in Fig. 5.4a and shows a maximum during July with an average value of 304±514 $m^3s^{-1}km^{-1}$ (Table 5.2) matching one of the highest water temperatures (Fig. 5.4b) since it accompanies the period of highest solar radiation during summer. This occurs right after achieving a minimum of FCO_2 during Spring, both in the Ria and Off-shore (Figs. 5.2 and 5.3), that corresponds to the period when in the Inner zone the waters start to behave as a source. NEP starts to increase in July too, having a delay of two months relative to the maximum upwelling except in the Ocean Zone. There, the peak of NEP occurs in April which coincided with the maximum values of seawater acting as a sink.

The maximum downwelling, expressed by negative values that occurred, during Winter coincides with the period of lower temperatures, with an average value of -436±1153 $m^3s^{-1}km^{-1}$ (Table 5.2), when there is the minimum NEP both in the Ría and Off-shore (Figs. 5.2 and 5.3).

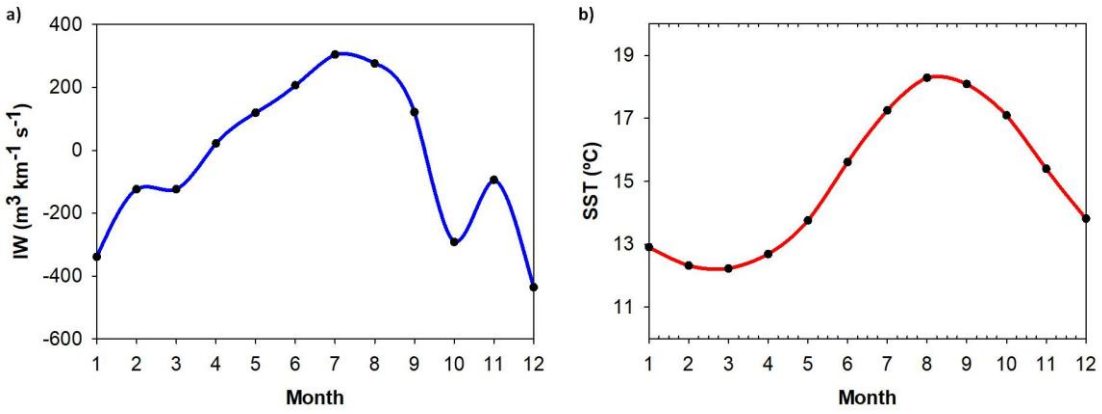

Figure 5.4: (a) upwelling index monthly average from 1997 to 2018, (b) SST (°C) used to make the calculations of the upwelling index monthly average from 1997 to 2018.

Table 5.2

Monthly average from 1997 to 2018 for the upwelling index and SST.

MONTH	IW (m^3 km^{-1} s^{-1}) ± SD	SST (°C) ±SD
1	-339±1143	12.90±0.46
2	-124±1024	12.32±0.47
3	-124±995	12.23±0.58
4	22±869	12.69±0.63
5	119±721	13.75±0.73
6	207±624	15.62±0.84
7	304±514	17.25±0.69
8	276±620	18.29±0.56
9	121±661	18.09±0.64
10	-292±978	17.09±0.74
11	-94±1107	15.40±0.82
12	-436±1153	13.81±0.55

The Figs. 5.5a and 5.5b relative to wind stress and SST for the months between1997 and 2017 from April to September are done with the same units and in the same format as Bakun did in 1990, for comparison of results. As it is possible to observe in Fig. 5.5a, during the spring and summer seasons, when upwelling is more intense since 2008, the differences between the annual averages of extremes of wind stress increased. However, Wind Stress along the years is showing a trend to decrease despite not significant (Table 5.3), as the pattern of SST (Table 5.3). which contradicts the Bakun theory. These figures just consider data from 1997 to 2017 because 2018 did not finish yet and it could influence the tendency.

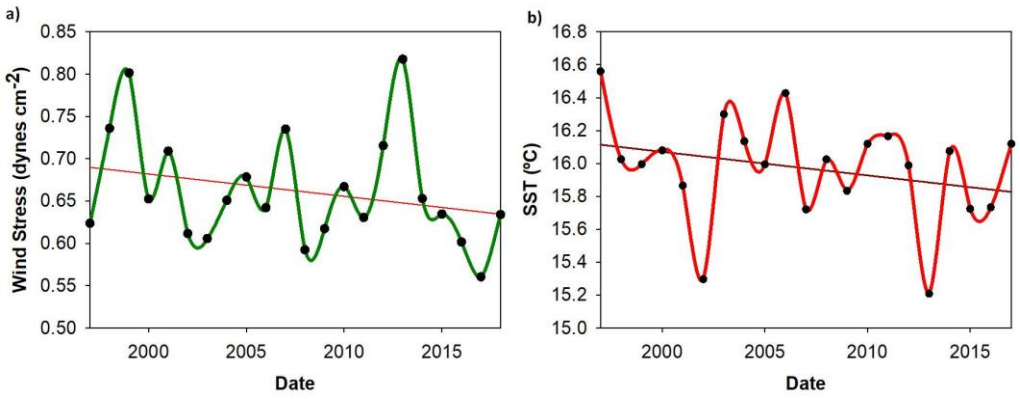

Figure 5.5: (a) Wind Stree and (b) SST between 1997 and 2017 but only for months between April and September (Spring and Summer).

Table 5.3

Statistical values from regression line for both Wind Stress and SST during Spring and Summer.

	Wind Stress (dynes cm^{-2})	SST (°C)
R^2	0.07	0.19
Intersect	0.9464	17.511
Slope	-0.003	-0.04

5.2.3 Long-Term Variability

Figure 5.6 represents the difference between fCO_2^{sw} and fCO_2^{atm} from 1997 to 2018 using the data from the campaigns having some gaps during the moments when there were no campaigns. It is possible to observe an increase in the Ria mainly during 2018. This increase is also observed in the Off-shore despite not so markedly. ΔfCO_2 is higher inside the Ria than off-shore, which could be explained by the shallowness and restriction of circulation inside the Ria in comparison with Off-shore, where the variability is more moderate.

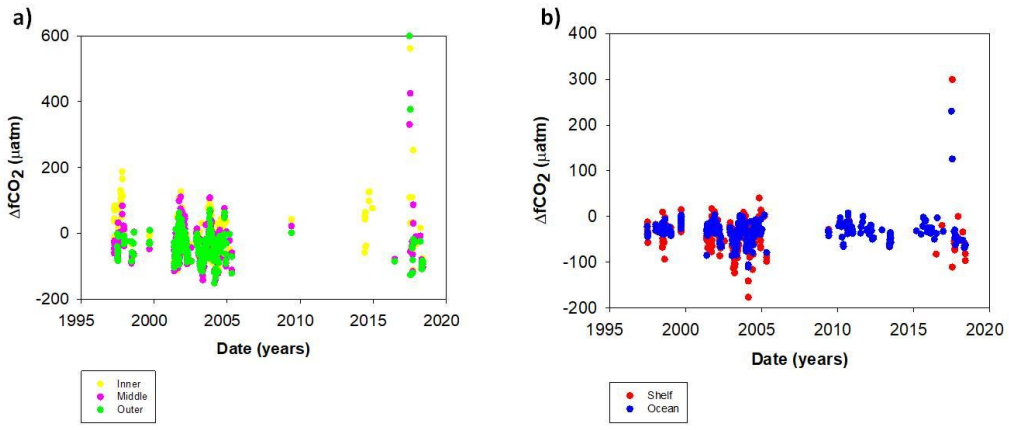

Figure 5.6: a) ΔfCO_2 daily average for Inner, Middle and Outer zones in yellow, pink and green respectively, (b) ΔfCO_2 daily average for the Shelf and the ocean in red and blue respectively.

Fig. 5.7 shows a daily average of the CO_2 flux acting both inside the Ria and Off-shore more as a sink than as a source, since a long time there is a trend to achieve more negative values, having differences with Fig. 5.6, where, due to the solubility and the CO_2 gas transfer velocity which gives to the off-shore values less potential of the waters

as a source. There is an intensification of a trend along the years both in the Ria and Off-shore, acting seawater more intensively as a sink of CO_2, particularly after 2010. On the Inner Ria, it is possible to observe some yellow value acting as a source in line with Fig. 5.3 where FCO_2 achieve his maximum values as a source of the total study zone.

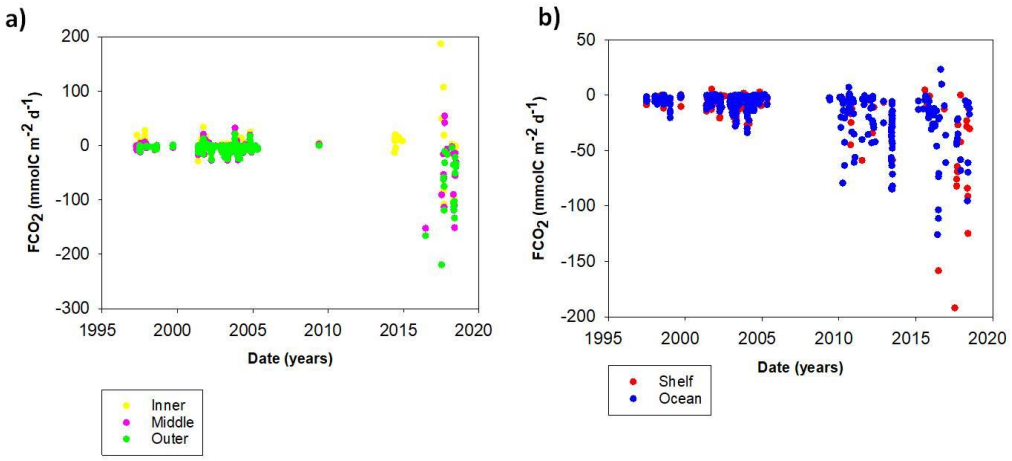

Figure 5.7: (a) FCO_2 daily average for Inner, Middle and Outer zones in yellow, pink and green respectively, (b) FCO_2 daily average for the Shelf and the ocean in red and blue respectively.

In Figs. 5.8c and 5.8d it can be observed that inside the Ria, NEP is higher than Off-shore. Between 2003 and 2009 there was a noticeable increase in the NEP regardless of the high variability in the upwelling index during these years (Fig. 5.8a). With these data is also possible to predict the seasonality of Net Ecosystem Production, showing that the periods of upwelling correspond to those of higher productivity, which corroborate the data presented in Figs. 5.2 and 5.3. In addition, it is noticeable that inside the Ria NEP is higher than Off-shore. This may be attributed to the shallowness of the Ría, where upwelled waters, enriched in nutrients in the photic zone, can promote more intense photosynthesis. Upwelling index was variable and mostly stable showing no tendency to increase or decrease (Fig. 5.8a)

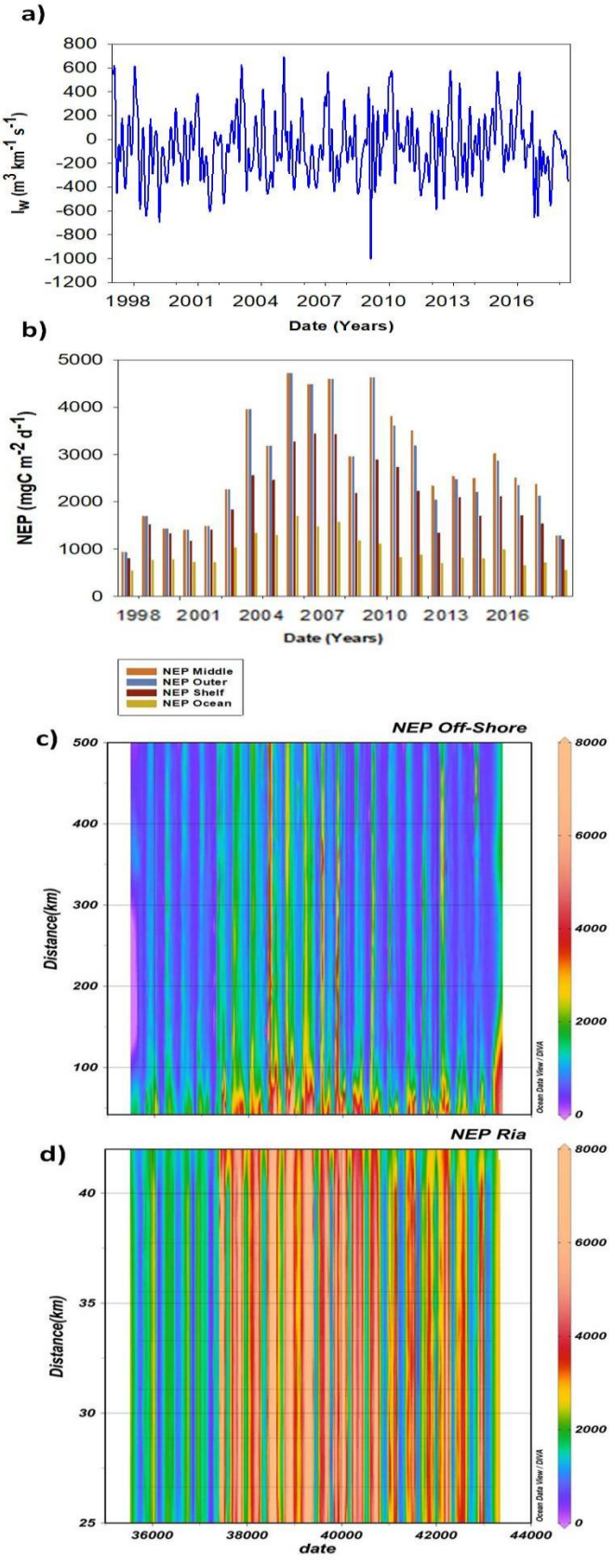

Figure 5.8: (a) Upwelling Index (m^3 km^{-1} s^{-1}) monthly average between 1997 to 2018, (b) NEP yearly average split by zones, (c) and (d) are NEP (mgC m^{-2} d^{-1}) daily average with the data interpolated having a global average in distance separated in Ria and Ocean respectively.

5.4 LONG TERM RELATIVE IMPORTANCE OF THE TEMPERATURE AND BIOLOGICAL EFFECTS ON fCO_2^{SW}

It is assumed that fCO_2^{SW} is influenced by two main processes. The first one due to biological processes such as photosynthesis and senescent phase which cause variability in the fCO_2^{SW}. The second factor is the temperature. To evaluate which one of these two components are dominant in each moment, it was used Equation 16 to evaluate the effect of the biological component and Equation 17 to evaluate the relative importance of seawater temperature.

In Fig. 5.9 it is possible to observe the values of fCO_2^{SW} indicated in a blue color, biological processes in green color and the temperature in red color. From this figure, it is possible to infer that most of the time, the biological component was the most relevant process, especially during the upwelling periods, while in winter the temperature component was more important. Most of the time, both components are opposite to each other i.e. the decrease in temperatures is compensated by biological utilization. Since 2014, both components seem to increase, the biological component especially in 2017, while the temperature component seems to be more intense in 2015 driving the behavior of fCO_2^{SW} along this year.

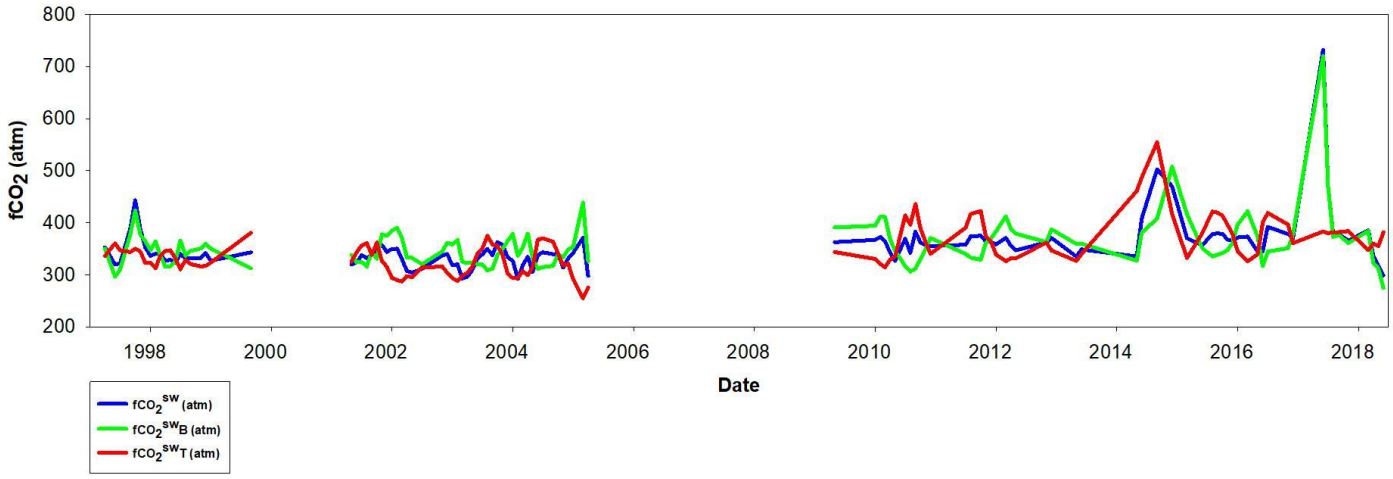

Figure 5.9 fCO_2^{SW} and their two components, the $fCO_2^{SW}B$ which is the biological component and the $fCO2^{SW}T$ which is the temperature component monthly average from 1997 to 2018.

The values in Fig. 5.10 show the combined effect of both components, biological and temperature, resulting in the net of fCO_2^{sw}. $fCO_2^{sw}B$ leads the behavior of fCO_2^{sw} more than the $fCO_2^{sw}T$, most part of the years, particularly in the Inner zone, while reducing its influence progressively with the increasing distance from the continent. The $fCO_2^{sw}B$ reached the maximum phytoplankton absorption during June inside the Ría with values around -80 µatm, -75 µatm and -60 µatm for the Inner, Middle, and Outer Ria, respectively. In the shelf and in the ocean the maximum absorption values occurred during Summer and Autumn with values lower than -50 µatm. During Winter there is a reversal in the behavior of $fCO_2^{sw}B$ with positive maximum values during January in the Ria above 100 µatm in the Inner and Middle zones, and 90 µatm in the Outer zone, from what it can be inferred that heterotrophic processes were dominant. In the Off-shore again the higher values of $fCO_2^{sw}B$ occurred during winter but with much more lower values than in the Ria. For all the study areas, in Autumn the warming temperatures contribute to increasing the weight in the fCO_2^{sw} net. It reached the maximum during September and October, achieving values around 25 µatm in the whole area agreeing right after the peak of upwelling (Fig. 5.4).

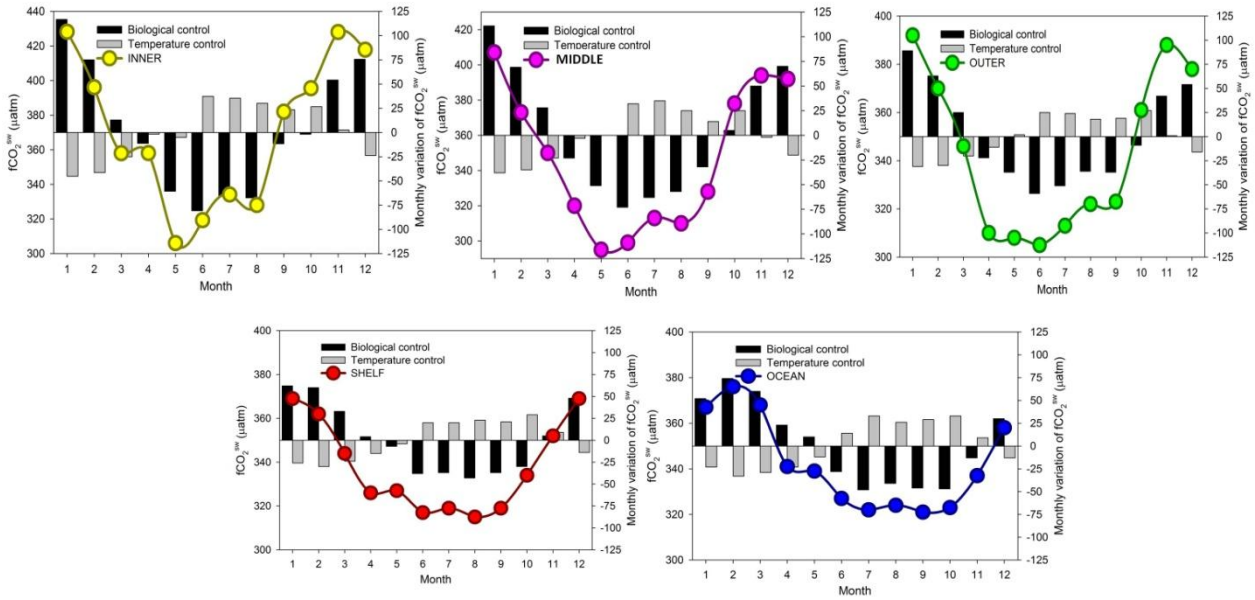

Figure 5.10: Data of net fCO_2^{sw} values for each zone (Inner, Middle, Outer, Shelf, and Ocean), showing the monthly average values from 1997 to 2018 indicated by the line, in black bars the $fCO_2^{sw}B$ (biological component) and in white bars the $fCO_2^{sw}T$ (temperature component).

5.5 SEASONAL fCO2sw VARIABILITY IN THE GALICIAN UPWELLING SYSTEM

The seasonal fCO_2^{sw} variability showed a multimodal pattern with several seasonal peaks towards the ocean (Fig. 5.11). The seasonal phases were opposite, the minimum and maximum values occurred during Spring and Autumn respectively. All the zones presented a clear seasonal pattern with minimum values in Spring and maximum values in Summer.

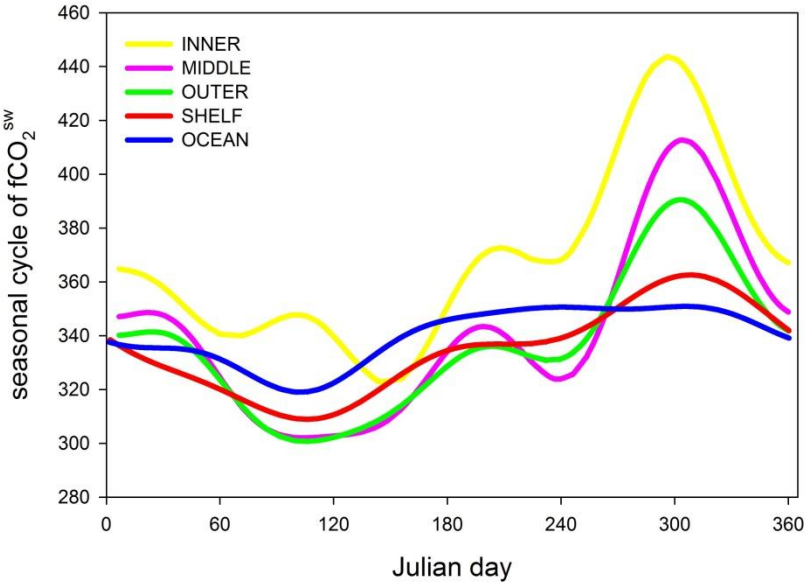

Figure 5.11: Seasonal fCO_2^{sw} variability.

In Table 5.4 the four harmonics do not explain more than 50% of the adjusted fCO_2^{sw} variability in each zone. Negative anomalies of SST, which are associated with the upwelling, show an increase in relation to fCO_2^{sw} in the Ria. Positive anomalies of SST has less weight over the fCO_2^{sw} than the negative anomalies in the Ria, promoting an important weight only in the ocean zone 8±3 µatm. The positive SSS coefficient leads to the presence of upwelled waters. The impact was higher in the ocean zone increasing from the middle to the ocean until 20±3 µatm. Chl*a* shows an inverse trend, with the Inner zone recording the greatest r^2 of 13%. The trend of interannual variability presents low weight.

Table 5.4

Regression coefficients for each predictor variable considered in the multiple linear regression (MLR) model adjusted to the mean fCO_2^{sw} values. r^2 is the percentage of normalized fCO_2^{sw} variability explained by SST (positive and negative anomalies), SSS, Chl*a*, and fCO_2^{sw} trend ($tfCO_2$). Root Mean Square Error (RMSE) and correlation coefficients (r^2), including the corresponding to the seasonal cycle (r^2), are also given ($p<0.05$).

	fCO_2	rmse	r^2	r^2SS	p-to-p	SST<0	r^2	SST>0	r^2	SSS	r^2	Chla	r^2	$tfCO_2$	r^2
INNER	368±6	35	53	30	125	-16±7	10					-5±1	13		
MIDDLE	340±3	31	65	45	112	-11±4	5	7±3	5	4±2	4	-2±1	5	2.4±0.8	1
OUTER	334±3	27	64	42	91	-10±3	3			8±2	10	-4±1	8	2.1±0.5	1
SHELF	333±2	19	64	34	55					13±2	24	-4±1	5	1.9±0.3	2
OCEAN	340±1	10	70	30	34			8±3	12	20±3	15	-5±2	7	2.3±0.4	2

5.6 CORRELATIONS WITH NAO DATA

With the aim of observing if there are some relationships between the studied variables between 1997 and 2018 and the NAO (which is an index based on a difference of atmospheric pressure centers that controls the direction of westerly winds) it was done a correlation for the variables SST, SSS, ΔfCO_2, FCO_2, Chl*a*, I_w, NAO Index, and Winter NAO. The data was split into two groups, Ría de Vigo and Off-shore (Tables 5.5 and 5.6). This was done because inside Ria de Vigo, the conditions change rapidly as indicated before, due to the shallowness and proximity to the continental zone, while in the Off-shore zone, the conditions are more stable. If these areas were not considered separately may conduct to erroneous conclusions.

5.6.1 Ria de Vigo

In Table 5.5, it is possible to observe the correlations between the studied variables for the Ria de Vigo, with NAO Index and winter NAO index monthly average values. NAO index and Winter NAO Index are inversely correlated with SST and SSS respectively. The stronger correlation was found between ΔfCO_2 and FCO_2 as expected, due to the small difference between them since the gas transfer velocity and the

solubility of CO_2 in the seawater are used to calculate FCO_2. Upwelling index inside the Ria is also correlated with SST and SSS.

Table 5.5

correlation between SST (ºC), SSS, ΔfCO_2 (atm), FCO_2 (mmolC m^{-2} d^{-1}), CHL*a*, Iw (m^3 km^{-1} s^{-1}), NAO Index, Winter NAO in Ria de Vigo.

		SST	SSS	ΔfCO_2	FCO_2	CHL*a*	Iw	NAO Index	Winter NAO
SST	Pearson	1	0.02	0.03	-0.03	-0.05	**0.19**	**-0.13**	0.1
SSS	Pearson	0.02	1	**0.15**	0.03	-0.08	**0.13**	-0.03	**-0.22**
ΔfCO_2	Pearson	0.03	**0.15**	1	**0.71**	**-0.15**	0.03	**-0.12**	-0.09
FCO_2	Pearson	-0.03	0.03	**0.71**	1	-0.13	0.01	-0.01	-0.03
CHL*a*	Pearson	-0.05	-0.08	**-0.15**	**-0.13**	1	0.04	-0.08	**0.14**
Iw	Pearson	**0.19**	**0.13**	0.03	0.01	0.04	1	0.06	-0.01
NAO Index	Pearson	**-0.13**	-0.03	-0.12	-0.01	-0.08	0.06	1	**0.25**
Winter NAO	Pearson	0.1	**-0.22**	-0.09	-0.03	0.14	-0.01	**0.25**	1
	N	757	757	757	757	557	757	757	757

5.6.2 Off-shore

In Table 5.6, for the Off-shore region, it is possible to observe that the relation between the NAO Index and Winter NAO, is higher than in the Ria, inversely correlated too with SST and SSS, respectively. Chl*a* has a strong negative correlation with SST which means that the highest Chla were associated with the lower SST suggesting the occurrence of upwelling.

The most important correlations are, ΔfCO_2 which is positively correlated with SST and negatively correlated with Chl*a* corroborating the results are drawn in Fig. 5.8.

Table 5.6

Off-Shore correlation between SST (ºC), SSS, ΔfCO_2 (atm), FCO_2 (mmolC m^{-2} d^{-1}), CHL*a*, Iw (m^3 km^{-1} s^{-1}), NAO Index, Winter NAO.

		SST	SSS	ΔfCO_2	FCO_2	CHL*a*	Iw	NAOIndex	WinterNAO
SST	Pearson	1	-0.01	**0.29**	0.05	**-0.3**	**0.13**	**-0.23**	0.04
SSS	Pearson	-0.01	1	0.1	-0.11	-0.4	-0.05	-0.07	**-0.25**
ΔfCO_2	Pearson	**0.29**	0.1	1	**0.77**	**-0.31**	0.01	-0.11	-0.06
FCO_2	Pearson	0.047	-0.11	**0.77**	1	-0.03	0.02	-0.00	0
CHL*a*	Pearson	**-0.30**	**-0.4**	**-0.31**	-0.03	1	0.05	0.05	0.03
Iw	Pearson	**0.13**	-0.05	0.01	0.02	0.05	1	-0.05	-0.04
NAO Index	Pearson	**-0.23**	-0.07	**-0.11**	-0.001	0.05	-0.05	1	**0.37**
Winter NAO	Pearson	0.04	**-0.25**	-0.065	0	0.03	-0.04	**0.37**	1
	N	798	787	787	787	636	798	798	798

6. DISCUSSION

6.1 SEASONAL VARIABILITY

Coastal upwelling systems in the Atlantic ocean are known to be sinks of atmospheric CO_2 while in the Pacific and Indian oceans they act as a source (Laurelle *et al*., 2010).

Ria de Vigo acts as a positive partially mixed estuary, with water that incomes from the ocean into the Ria along the bottom, with saltier waters enriched in nutrients due to remineralization processes (Alvalez-Salgado *et al*., 1993). This process of remineralization of the material inside the Ria provokes the Ría becoming a sink of CO_2 (Álvarez-Salgado *et al*., 1993) transforming CO_2 in the form of organic matter again into inorganic CO_2 due to microbes community (Cavan *et al*., 2017), as it was possible to observe in Spring months (Fig. 5.2 and 5.3) with a peak on May. Under downwelling condition (Fig. 5.4), there is a reversal in the estuarine circulation, with the upwelled water being evacuated through the bottom of the Ría. It generates a high flux of sediment outside the Ría to the shelf. This process contributes to the regeneration of carbon and nutrients in the water column, by the oxidation of suspended particulate organic carbon (Diz *et al*., 2006). The values of SSS higher than 30 (Fig. 5.2, Table 5.1), can be indicative that most part of the waters from the Ría are mainly from a marine origin (Doval *et al*., 2016), except during downwelling periods. These, mostly occur in the winter season, when less salty waters prevail. SSS is lower inside Ria de Vigo achieving values of 30.09±3.69 in the Inner zone (Table 5.1), which is in agreement with Pérez *et al*. (1999) and Sousa *et al*. (2014) that explained that due to an important runoff of freshwater coming into the Ria during high river discharges and under southerlies, the Ria shows an important decrease in salinity. This period corresponds to downwelling, which does not allow a spreading of the freshwater off-shore. The run-off of freshwater creates a marine stratification which generally occurs in highly freshwater discharge systems (Laurelle, *et al*., 2010).

Comparing the thesis done before (Cobo *et al*., 2014) with the data from 1997 to 2009 the same behavior as found in Fig. 5.4 was achieved. From 1997 to 2009 the values were higher than 500 $m^3\ km^{-1}\ s^{-1}$ while between 1997 to 2018 the maximum value does not achieve 400 $m^3 km^{-1} s^{-1}$. The values in Fig. 5.4 corroborate the trend of Fig. 5.5, where the wind stress tends to decrease like the upwelling itself.

Data from 1997 to 2009 for Figs. 5.2 and 5.3, in general terms, have the same behavior that during 1997 to 2018, except in the Shelf (Fig. 5.3), where the peak in NEP moves from April, as found in the work done before to August, like in the Middle and Outer Ria (Figs. 5.2 and 5.3). In general terms, NEP increases during the period from 1997 to 2018 compared with data reported by Cobo *et al*. (2014).

Off-shore, seawater acts as a sink of CO_2 most part of the year, with the maximum exchange values during March and April as observed in Fig. 5.3. This means that globally the whole zone, in average, acts as a sink of CO_2 contributing to the global air-to-sea CO_2 fluxes as the west coasts of North America, South America, and South Africa (Hales *et al*., 2005). The outgassing from seawater of CO_2 (Figs. 5.2 and 5.3) is increasing directly at the end of the upwelling period inside the Ria. If the upwelling would increase as Bakun (1990) theorized, this might promote an increase in the outgassing of the CO_2 to the atmosphere, that depends on other factors, such as temperature and biological processes. It is important to take into account that the use of reduced sampled surface areas can lead to an overestimation of the sinking value of CO_2 (Laurelle, *et al*., 2010). The CO_2 outgassing, especially in the Inner zone in the Ría (Fig. 5.2), can be caused by upwelling (Fig. 5.4), but enhanced by the rapid heating of the water due to the shallowness of the waters in this area, that can get easily warmed up relatively to off-shore during the summer season as reported by Torres *et al*. (2011), for this region. NEP can be related with upwelling periods, but it is also influenced by the runoff of the river plume (Figs. 5.2 and 5.3), as referred by Sousa *et al*., (2014). Hence, higher rates of NEP starts to develop during September matching the maximum exchange of CO_2^{sw} to the atmosphere, and having $fCO_2^{sw}B$ negative (Fig. 5.10), possibly because of the increase of photosynthetic activity. Primary production rates in coastal upwelling areas are higher than off-shore because the enhanced horizontal fluxes in organic matter export from upwelling zones are more effective (Álvarez-Salgado *et al*., 2000). For this reason, NEP is almost twice times higher in the Middle and Outer zones than in the shelf and the ocean (Figs. 5.2 and 5.3). NEP start to decrease during downwelling periods starting in October and achieving the minimum during December and January. These rates are higher under extreme cases when Eastern North Atlantic Central Waters (ENACW) reaches the photic layer. This will cause an increase in primary productivity where the Ria de Vigo act as a nutrient trap and a source of atmospheric CO_2, as supported by Fig. 5.10 where $fCO_2^{sw}B$ dominates over $fCO_2^{sw}T$.

Moreover, this suggests that heterotrophic processes caused high rates of carbon deposition from atmospheric CO_2 (Diz *et al*., 2006). These results also agree with those reported by Doval *et al*. (2016).

For every seasonal cycle, FCO_2 reached the lowest values during the spring phytoplankton bloom (Figs. 5.2 and 5.3) in accordance with the works of Pérez *et al*. (1999) and Gago *et al*. (2003). The low levels of FCO_2 generated by the spring bloom were maintained for some time in the water column while the Chl*a* disappeared through grazing and sinking (Pérez *et al*., 1999). The decrease in CO_2 generated by the bloom remained for some weeks while Chl*a* became degraded (Pérez *et al*., 1999).

6.2 LONG-TERM VALUES

FCO_2 daily values (Fig. 5.7) support the statement of Laurelle *et al*., (2010) referring that temperate and high latitudes (mostly in the northern hemisphere) in the continental shelf areas and estuarine environments are sinks for atmospheric CO_2, with a particular increase of this behavior in the last years.

The results from Fig. 5.9 on the biological component, are higher than 140 µatm, the values observed in high latitudes in the northern oceans around 40ºN as reported by Takahashi *et al*. (2002). These results confirm the seasonal signals and match a strong biological effect that is, generally, out of phase relative to temperature, (Fig. 5.10). The data are in accordance with those reported by Takahashi *et al*., (2002), that also found that the biology effect dominates over temperature effect, for both hemispheres in high latitudes. Lohrenz & Cai (2006), for the Gulf of Mexico, conducted a principal component analysis of SSS, SST, and Chl*a* and found that these parameters explain 98% of the variation of the pCO_2 in the ocean. The same kind of results are reported by Takahashi *et al*. (2002), that show that the variation of pCO_2, depends mostly on two components, one biological and one physical (SST). These data also show that the long-term variability in upwelling systems is coupled to changes in the ecosystem productivity (Figs. 5.9 and 5.10) and may influence the frequency of harmful algal blooms (Pérez *et al*., 2010).

Data from the seasonal cycle show values similar to those reported before by Cobo *et al*. (2014) between 1997 and 2009. In this case, I_w was not significant for any of the studied zones. Even though its effect is already explained by SST and Chl*a*. SST

anomalies were lower than in other regions as California (Cobo *et al*., 2014). The interannual trend continues to be not important, maybe the time period should be longer to find some cyclicity (Cobo *et al*., 2014).

In this study, monthly NAO is not correlated with I_w (Tables 5.5 and 5.6) in opposition to Perez *et al*. (2010) that found a positive significant correlation between both variables. This is important because the highest values of NAO Index leads to an increase in the westerly winds which could intensify I_w, as well as the Ekman Transport that is directly related to wind variable. However, monthly NAO is negatively correlated with SST, at the same time is positively correlated with I_w. That relation between I_w and NAO Index is achieved indirectly through the connection with SST as found by Pérez *et al*. (2010). Furthermore, like in the data from Table 5.5 and 5.6, Visbeck *et al*. (2001) found that NAO is related to SST that vary significantly with the overlying atmosphere.

In Table 5.6, it was observed a strong relationship between SST and Chl*a* with ΔfCO_2, confirming that both variables are important parameters to explain ΔfCO_2 functioning as referred by Takahashi *et al*. (2002) and Lohrenz & Cai (2006),.

6.3 BAKUN'S THEORY

Bakun (1990), theorized that in some regions including the Iberian Peninsula at 43° latitude the wind stress will be increasing during Spring and Summer, but this is not happening in the time series analyzed from 1997 to 2018 (Fig. 5.5). In fact, the wind stress is decreasing. This theory was based on the higher differences in the temperature between the continent and the ocean that would develop an increase in the intensity of the wind. Correspondently, this would increase the Ekman transport and produce an increment in the upwelling intensity. However, this is not the case what is in line with the data analyzed by Relvas *et al*. (2009), for Portugal.

Data for the region of Galician coast analyzed by Perez *et al*. (2010) and satellite data for the region of Portugal coast (Leixões zone) analyzed by Relvas *et al*. (2009) show that there is a tendency of SST to increase from 1992 to 2008 and 1985 to 2005, respectively. However, in this study, there is a decrease in the summer annual temperature averages. This could be explained by Lemos & Pires (2004) who indicate that there is an increasing warming in the SST while the latitude decrease. Another answer to that could be that during the Spring and Summer months SST is decreasing

but in Winter SST could be warmer. This could be one aspect that is important to take into account for further studies.

As a consequence of the decrease in the SST, the FCO_2 modify its pattern, becoming more frequently a sink of CO_2 (Fig. 5.7). This causes changes in the Ria with an increasing trend of being a sink of CO_2. Of course, it is important to take into account the strange behavior of SST of these data taken from NCEP/NCAR which shows a tendency to decrease. Nevertheless, Wiltshire & Manly (2004) report that for the North Sea it is possible to infer a cyclicity of at least 10 to 20 years, where between 1870 to 1890, and 1970 to 1985 it is possible to observe that the SST average tendency decreased while between 1985 to 2000 the tendency of the average SST increased. Moreover, the same authors considering the period between 1962 and 2002, and more specifically the same range of time of the present study, the SST trend increased. It would be important to study a larger range of data to determine the real tendency of the SST.

There is another important variable, recognized as the most significant pattern of climate variability in the North Atlantic Sector, that Bakun did not take into account which is the NAO. It is related with SST (Table 5.6) and controls the westerly winds, but there are a lot of uncertainties about how is changing according to the increase of the greenhouse gasses (Visbeck *et al*., 2003).

6.4 WEAKNESSES IN THE DATA

6.4.1 Campaigns

Most of the campaigns were done during the night, this can mean an important difference in the daily CO_2 exchange, due to, during the day the zones have a tendency towards a sink while during the night the zones have a tendency as a source, mainly due to phytoplankton blooms (Frankignoulle, 1988). In consequence, to compare the data it is important first knowing the time of the day when there are being done the measurements. Further, to upwelling act as a source or a sink, it does not depend on the upwelling itself but also on the present stage of the bloom. If upwelling happens when there is a low population of microbial activity there will be a phytoplankton bloom and less respiration from these microbes that can fix CO_2. However, if there is a high population of microbes when there is upwelling, it will develop, due to respiration, an

outgassing area (Jiao *et al*., 2014). This is important because of the relationship between the NEP taken from satellites sources and data of CO_2 exchange taken from different sources.

6.4.2 Calculations

pCO_2 normally has an error because pH is taken with constant temperature, that is important to correct with the SST. A drift in the measure of the SSS could increase the error in these calculations of pCO_2, as found by Williams *et al*. (2017). In this study, it was paid attention to calculate the pCO_2 having in account the SST in each moment, at least for the ARIOS campaign between 2017 and 2018. The largest source of uncertainty in calculating pCO_2(pH, TA) is the accuracy of the pH sensor measurements. Thus, the mean ΔpCO_2 is highly dependent on how the pH sensor is calibrated (Williams *et al*., 2017).

7. CONCLUSIONS

It is not noticed a decrease or increases in the upwelling index but what it is possible to conclude is that wind stress has a decreasing trend, contrary to what Bakun reported.

Both physical and biological components are important in the fCO_2^{sw}, having a strong negative correlation between Chl*a* and SST. It is possible to conclude that $fCO_2^{sw}B$ control the fCO_2^{sw} over $fCO_2^{sw}T$ except when upwelling appears taking $fCO_2^{sw}T$ advantage over $fCO_2^{sw}B$.

Even though it is not possible to observe any correlation between CO_2 exchange and Upwelling Index. There is a correlation between I_w and SST, and between ΔfCO_2 and SST, being SST a main component in the CO_2 exchange. However, in this case, the monitoring is a product of different projects which are not synchronic in time.

There is an increase in the NEP mostly since 2006, with a peak in 2009, and decreasing again since 2010. This could infer a cyclicity that should not be related with NAO Index. An answer to this question could be given by future works with greater availability of data.

8. REFERENCES

Álvarez-Salgado, X. A., Rosón, G., Pérez, F. F, and Pazos, Y. (1993). Hydrographic Variability off the Rías Baixas (NW Spain) During the Upwelling Season. *Journal of Geophysical Research 98(C8)*:14447–14455**.**

Álvarez-Salgado, X. A., Beloso, S., Joint, I., Nogueira, E., Chou, L., Pérez, F. F., Groom, S., Cabanas, J.M., Rees, A.P, and Elskens, M. (2002). New production of the NW Iberian shelf during the upwelling season over the period 1982-1999. *Deep-Sea Research Part I: Oceanographic Research Papers*, *49*(10), 1725-1739. doi:10.1016/S0967-0637(02)00094-8

Álvarez-Salgado, X. A., Doval, M. D., Borges, A. V., Joint, I., Frankignoulle, M., Woodward, E. M. S. and Figueiras, F. G. (2001). Off-shelf fluxes of labile materials by an upwelling filament in the nw Iberian upwelling system. *Progress in Oceanography, 51*(2-4), 321-337. doi:10.1016/S0079-6611(01)00073-8

Álvarez-Salgado, X. A., Gago, J., Míguez, B. M., Gilcoto, M. and Pérez, F. F. (2000). Surface waters of the NW Iberian margin: Upwelling on the shelf versus outwelling of upwelled waters from the Rías Baixas. *Estuarine, Coastal and Shelf Science, 51*(6), 821-837. doi:10.1006/ecss.2000.0714

Álvarez-Salgado, X. A., Labarta, U., Fernández-Reiriz, M. J., Figueiras, F. G., Rosón, G., Piedracoba, S., Filgueira, R. and Cabanas, J. M. (2008). Renewal time and the impact of harmful algal blooms on the extensive mussel raft culture of the Iberian coastal upwelling system (SW Europe). *Harmful Algae*, *7*(6), 849-855. doi:10.1016/j.hal.2008.04.007

Alvarez, I., Ospina-Alvarez, N., Pazos, Y., deCastro, M., Bernardez, P., Campos, M. J., Gomez-Gesteira, J.L., Alvarez-Ossorio, M.T., Varela, M., Gomez-Gesteira, J.L. and Prego, R. (2009). A winter upwelling event in the Northern Galician Rias: Frequency and oceanographic implications. *Estuarine, Coastal and Shelf Science*, *82*(4), 573-582. doi:10.1016/j.ecss.2009.02.023

Arístegui, J., Álvarez-Salgado, X. A., Barton, E. D., Figueiras, F. G., Hernández-León, S., Roy, C. and Santos, A. M. P. (2006). Oceanography and fisheries of the Canary current - Iberian region of the eastern North Atlantic. *The Sea, 14B*, 877-932.

Arístegui, J., Barton, E. D., Álvarez-Salgado, X. A., Santos, A. M. P., Figueiras, F. G., Kifani, S., Hernández-León, S., Mason, E., Machú, E. and Demarcq, H. (2009). Sub-regional ecosystem variability in the Canary Current upwelling. *Progress in Oceanography*, *83*(1-4), 33-48. doi:10.1016/j.pocean.2009.07.031

Bakun, A. (1973) Coastal upwelling indices, west coast of North America 1946– 1971. *NOAA Technical Report*, NMFSSSRF-671, 103 pp.

Bakun, A. (1990). Global Climate Change and Intensification of Coastal Ocean Upwelling. *Science 247(4939)*:198–201.

Bakun, A. and Weeks, S. J. (2004). Greenhouse gas buildup, sardines, submarine eruptions and the possibility of abrupt degradation of intense marine upwelling ecosystems. *Ecology Letters*, *7*(11), 1015-1023. doi:10.1111/j.1461-0248.2004.00665.x

Barton, E. D., Field, D. B. and Roy, C. (2013). Canary current upwelling: More or less? *Progress in Oceanography*, *116*, 167-178. doi:10.1016/j.pocean.2013.07.007

Behrenfeld, M. J., and Falkowski, P. G. (1997). Photosynthetic rates derived from satellite-based chlorophyll concentration. *Limnology and Oceanography 42(1)*:1–20.

Blanton, J., Tenore, K., Castillejo, F., Atkinson, L., Schwing, F. and Lavin, A. (1987). Relationship of upwelling to mussel production in the Rias on the western coast of Spain. *Journal of Marine Research*, *45*(2), 497-511. doi:10.1357/002224087788401115

Borges, A. V. and Frankignoulle, M. (2001). Short-term variations of the partial pressure of CO2 in surface waters of the Galician upwelling system. *Progress in Oceanography*, *51*(2-4), 283-302. doi:10.1016/S0079-6611(01)00071-4

Borges, A. V. and Frankignoulle, M. (2002). Aspects of dissolved inorganic carbon dynamics in the upwelling system off the Galician coast. *Journal of Marine Systems*, *32*(1-3), 181-198. doi:10.1016/S0924-7963(02)00031-3

Borges, A. V., Delille, B. and Frankignoulle, M. (2005). Budgeting sinks and sources of CO2 in the coastal ocean: Diversity of ecosystems counts. *Geophysical Research Letters 32(L14601):*4pp.

Cai, W.J. (2011). Estuarine and Coastal Ocean Carbon Paradox: CO_2 Sinks or Sites of Terrestrial Carbon Incineration? *Annual Review of Marine Science*, *3*(1), 123-145. doi:10.1146/annurev-marine-120709-142723

Casey, K. S. and Cornillon, P. (2001). Global and Regional Sea Surface Temperature Trends. *Journal of Climate, 14*(18), 3801-3818. doi:10.1175/1520-0442(2001)014<3801:GARSST>2.0.CO;2

Cavan, E. L., Trimmer, M., Shelley, F. and Sanders, R. (2017). Remineralization of particulate organic carbon in an ocean oxygen minimum zone. *Nature Communications*, *8*(May 2016), 1-9. doi:10.1038/ncomms14847

Chavez, F. P., Pennington, J. T., Castro, C. G., Ryan, J. P., Michisaki, R. P., Schlining, B., Waltz, P., Buck, K.R., McFadyen, A. and Collins, C. A. (2002). Biological and chemical consequences of the 1997 – 1998 El Niño in central California waters. *Progress in Oceanography*, *54*, 205-232. doi:10.1016/s0079-6611(02)00050-2

Clayton, T. D. and Byrne, R. H. (1993). Spectrophotometric seawater pH measurements: total hydrogen ion concentration scale calibration of m-cresol purple and at-sea results. *Deep-Sea Research*, *40*, 2115-2129.

Cobo-Viveros, A. M., Padin, X. A., Otero, P., De la Paz, M., Ruiz-Villarreal, M., Ríos, A. F. and Pérez, F. F. (2013). Short-term variability of surface carbon dioxide and sea-air CO2 fluxes in the shelf waters of the Galician coastal upwelling system. *Scientia Marina, 77*(S1), 37-48. doi:10.3989/scimar.03733.27C

Cobo-Viveros, A. (2014). CO2 Flux variability in the Galician and California Upwelling Systems. *PHD Thesis. CSIC.* pp: 113-140.

Dickson, A. G., Sabine, C. L. and Christian, J. R. (2007). Guide to best practices for ocean CO2 measurements. Issue 8 of the IOCCP report. Issue 3 of PICES special publication. *PICES Special Publication 3.*

Diz, P., Francés, G. and Rosón, G. (2006). Effects of contrasting upwelling-downwelling on benthic foraminiferal distribution in the Ría de Vigo (NW Spain). *Journal of Marine Systems*, *60*(1-2), 1-18. doi:10.1016/j.jmarsys.2005.11.001

Doval, M. D., López, A. and Madriñán, M. (2016). Temporal variation and trends of inorganic nutrients in the coastal upwelling of the NW Spain (Atlantic Galician rías). *Journal of Sea Research, 108*, 19-29. doi:10.1016/j.seares.2015.12.006

Etheridge, D. M., Steele, L. P., Langenfelds, R. L., Francey, R. J., Barnola, J. M. and Morgan, V. I. (1996). Natural and anthropogenic changes in atmospheric CO2 over the last 1000 years from air in Antartic ice and firn. *Journal Of Geophysical Research-Atmospheres*, *101*(D2), 4115-4128. doi:10.1029/95JD03410

Frankignoulle, M. (1988). Field measurements of air-sea CO2, exchange. *Limnology and Oceanography Limnol. Oceanogr, 33*(3), 3-13.

Fung, I. Y., Doney, S. C., Lindsay, K. and John, J. (2005). Evolution of carbon sinks in a changing climate. *Proceedings of the National Academy of Sciences of the United States of America*, *102*(32), 11201-11206. doi:10.1073/pnas.0504949102

Gago, J., Gilcoto, M., Perez, F. E. and Rios, A. F. (2003). Short-term variability of fCO2 in seawater and air-sea CO2 fluxes in a coastal upwelling system (Ria de Vigo, NW Spain). *Marine Chemistry, 80*, 247-264.

García-Reyes, M., Largier, J. L. and Sydeman, W. J. (2014). Synoptic-scale upwelling indices and predictions of phyto and zooplankton populations. *Progress in Oceanography, 120*, 177-188. doi:10.1016/j.pocean.2013.08.004

Hales, B., Takahashi, T. and Bandstra, L. (2005). Atmospheric CO_2 uptake by a coastal upwelling system. *Global Biogeochemical Cycles*, *19*(1), 1-11. doi:10.1029/2004GB002295

Herrera, J. L., Piedracoba, S., Varela, R. A. and Rosón, G. (2005). Spatial analysis of the wind field on the western coast of Galicia (NW Spain) from in situ measurements. *Continental Shelf Research*, *25*(14), 1728-1748. doi:10.1016/j.csr.2005.06.001

Hidy, G. M. (1972). A view of recent air-sea interaction research. *Bulletin of the American Meteorological Society 53(11)*:1083–1102.

Hurrel, J.W. (1995). Decadal trend in the North Atlantic oscillation regional temperatures and precipitation. *Science* 269, 676-679.

Jiao, N., Zhang, Y., Zhou, K., Li, Q., Dai, M., Liu, J., Guo, J. and Huang, B. (2014). Revisiting the CO2 « source » problem in upwelling areas – A comparative study on eddy upwellings in the South China Sea. *Biogeosciences*, *11*(9), 2465-2475. doi:10.5194/bg-11-2465-2014

Körtzinger, A., Thomas, H., Schneider, B., Gronau, N., Mintrop, L. and Duinker, J. C. (1996). At-sea intercomparison of two newly designed underway pCO2 systems encouraging results. *Marine Chemistry 52(2)*:133–145.

Lachkar, Z. and Gruber, N. (2013). Response of biological production and air-sea CO2fluxes to upwelling intensification in the California and Canary Current Systems. *Journal of Marine Systems*, *109-110*, 149-160. doi:10.1016/j.jmarsys.2012.04.003

Lamont, T., García-Reyes, M., Bograd, S. J., van der Lingen, C. D. and Sydeman, W. J. (2017). Upwelling indices for comparative ecosystem studies: Variability in the Benguela Upwelling System. *Journal of Marine Systems*. doi:10.1016/j.jmarsys.2017.05.007

Laruelle, G. G., Dürr, H. H., Slomp, C. P. and Borges, A. V. (2010). Evaluation of sinks and sources of CO2 in the global coastal ocean using a spatially-explicit typology of estuaries and continental shelves. *Geophysical Research Letters 37(L15607)*:6

Legendre, L., Rivkin, R. B., Weinbauer, M. G., Guidi, L. and Uitz, J. (2015). The microbial carbon pump concept: Potential biogeochemical significance in the globally changing ocean. *Progress in Oceanography*, *134*, 432-450. doi:10.1016/j.pocean.2015.01.008

Lemos, R. T. and Pires, H. O. (2004). The upwelling regime off the west Portuguese coast, 1941-2000. *International Journal of Climatology*, *24*(4), 511-524. doi:10.1002/joc.1009

Lewis, E., Wallace, D. and Allison, L. J. (1998). Program Developed for CO2 System Calculations. *Carbon Dioxide Information Analysis Center*, Upton, New York.

Liss, P. S. and Merlivat, L. (1986). Air-Sea Gas Exchange Rates: Introduction and Synthesis in Buat-Ménard, editor. The Role of Air-Sea Exchange in Geochemical Cycling. *Springer Netherlands.* 113–127

Lohrenz, S. E. and Cai, W. J. (2006). Satellite ocean color assessment of air-sea fluxes of CO2 in a river-dominated coastal margin. *Geophysical Research Letters*, *33*(1), 2-5. doi:10.1029/2005GL023942

McGillis, W. R., Edson, J. B., Hare, J. E. and Fairall, C. W. (2001). Direct covariance air-sea CO2 fluxes. *Journal of Geophysical Research: Oceans 106(C8)*:16729–16745.

McGregor, H. V., Dima, M.H., Fischer, W. and Mulitza, S. (2007). Rapid 20th-Century Increase in Coastal Upwelling off Northwest Africa. *Science 315(5812)*:637– 639.

Messié, M. and Chavez, F. P. (2015). Seasonal regulation of primary production in eastern boundary upwelling systems. *Progress in Oceanography*, *134*, 1-18. doi:10.1016/j.pocean.2014.10.011

Narayan, N., Paul, A., Mulitza, S. and Schulz, M. (2010). Trends in coastal upwelling intensity during the late 20th century. *Ocean Science*, *6*(3), 815-823. doi:10.5194/os-6-815-2010

Nightingale, P. D., Malin, G., Law, C. S., Watson, A. J., Liss, P. S., Liddicoat, M. I., Boutin, J. and Upstill-Goddard R. C. (2000b). In situ evaluation of air-sea gas exchange parameterizations using novel conservative and volatile tracers. *Global Biogeochemical Cycles 14(1)*:373–387.

Nogueira, E., Ibanez, F. and Figueiras, F. G. (2000). Effect of meteorological and hydrographic disturbances on the microplankton community structure in the Ria de Vigo (NW Spain). *Marine Ecology Progress Series*, *203*, 23-45. doi:10.3354/meps203023

Olsen, A., Bellerby, R. G. J., Johannessen, T., Omar, A. M. and Skjelvan, I. (2003). Interannual variability in the wintertime air-sea flux of carbon dioxide in the northern North Atlantic, 1981-2001. *Deep-Sea Research Part I: Oceanographic Research Papers*, *50*(10-11), 1323-1338. doi:10.1016/S0967-0637(03)00144-4

Otero, P., Padin, X. A., Ruiz-Villarreal, M., García-García, L. M. A., Ríos, F. and Pérez, F. F. (2013). Net sea-air CO2 flux uncertainties in the Bay of Biscay based on the choice of wind speed products and gas transfer parameterizations. *Biogeosciences 10(5)*:2993–3005.

Padin, X. A., Vázquez-Rodríguez, M., Rios, A. F. and Pérez, F. F. (2007). Atmospheric CO2measurements and error analysis on seasonal air-sea CO2fluxes in the Bay of Biscay. *Journal of Marine Systems*, *66*(1-4), 285-296. doi:10.1016/j.jmarsys.2006.05.010

Pardo, P. C., Padín, X. A., Gilcoto, M., Farina-Busto, L. and Pérez, F. F. (2011). Evolution of upwelling systems coupled to the long-term variability in sea surface temperature and Ekman transport. *Climate Research 48(2)*:231–246.

Pérez, F. F., Padín, X. A., Pazos, Y., Gilcoto, M., Cabanas, M., Pardo, P. C., Doval, M. D. and Farina-Busto, L. (2010). Plankton response to the weakening of the Iberian coastal upwelling. *Global Change Biology 16(4):*1258–1267.

Perez, F. F. and Fraga, F. (1987). A precise and rapid analytical procedure for alkalinity determination. *Marine Chemistry*, *21*(2), 169–182.

Pérez, F. F., Ríos, A. F. and Rosón, G. (1999). Sea surface carbon dioxide off the Iberian Peninsula (North Eastern Atlantic Ocean). *Journal of Marine Systems*, *19*(1-3), 27-46. doi:10.1016/S0924-7963(98)00022-0

Pond, S. and Pickard, G. (2016). Introductory Dynamical Oceanography. 2nd ed. Kent: *El sevier Science*, pp. 109-117.

Relvas, P., Luís, J. and Santos, A. M. P. (2009). Importance of the mesoscale in the decadal changes observed in the northern Canary upwelling system. *Geophysical Research Letters*, *36*(22), 2-5. doi:10.1029/2009GL040504

Siegenthaler, U. and Sarmiento, J. (1993). Atmospheric carbon dioxide and the ocean.

Nature, 365(6442), pp.119-125.

Simpson, J. J. and Zrino, A. (1980). Biological control of pH in the Peruvian coastal upwelling sea. *Deep-Sea Research, 27*, 733-743.

Sousa, M. C., Mendes, R., Alvarez, I., Vaz, N., Gomez-Gesteira, M. and Dias, J. M. (2014). Unusual circulation patterns of the Rias Baixas induced by Minho freshwater intrusion (NW of the Iberian Peninsula). *PLoS ONE*, *9*(11). doi:10.1371/journal.pone.0112587

Sousa, M. C., Vaz, N., Alvarez, I., Gomez-Gesteira, M. and Dias, J. M. (2014). Influence of the Minho river plume on the rias Baixas (nw of the Iberian peninsula). *Journal of Marine Systems*, *139*, 248-260. doi:10.1016/j.jmarsys.2014.06.012

Sweeney, C., Gloor, E., Jacobson, A. R., Key, R. M., McKinley, G., Sarmiento, J. L. and Wanninkhof, R. (2007). Constraining global air-sea gas exchange for CO2 with recent bomb 14C measurements. *Global Biogeochemical Cycles 21(2)*: GB2015.

Sydeman, W. J., García-Reyes, M., Schoeman, D. S., Rykaczewski, R. R., Thompson, S. A., Black, B. A. and Bograd, S. J. (2014). Climate change and wind intensification in coastal upwelling ecosystems. *Science*, *345*(6192), 77-80. doi:10.1126/science.1251635

Takahashi, T., Sutherland, S. C., Sweeney, C., Poisson, A., Metzl, N., Tilbrook, B., Bates, N., Wanninkhof, R., Feely, R.A., Sabine, C., Olafsson, J. and Nojiri, Y. (2002). Global sea-air CO_2 flux based on climatological surface ocean pCO_2, and seasonal biological and temperature effects. *Deep-Sea Research Part II: Topical Studies in Oceanography*, *49*, 1601-1622. doi:10.1016/S0967-0645(02)00003-6

Takahashi, T., Sutherland, S. C., Wanninkhof, R., Sweeney, C., Feely, R. A., Chipman, D. W., Hales, B., Friederich, G., Chavez, F., Sabine, C., Watson, A., Bakker, D.C.E., Schuster, U., Metzi, N., Yoshikawa-Inoue, H., Ishii, M., Midorikawa, T., Nojiri, Y., Körtzinger, A., Steinhoff, T., Hoppema, M., Olafsson, J., Arnarson, T.S., Tilbrook, B., Johannessen, T., Olsen, A., Bellerby, R., Wong, C.S., Delille, B., Bates, N.R. and de Baar, H. J. W. (2009). Climatological mean and decadal change in surface ocean pCO2, and net sea-air CO2flux over the global oceans. *Deep-Sea Research Part II: Topical Studies in Oceanography, 56*(8-10), 554-577. doi:10.1016/j.dsr2.2008.12.009

Torres, R., Pantoja, S., Harada, N., González, H. E., Daneri, G., Frangopulos, M., Rutlant, J.A., Duarte, C.M., Rúiz-Halpern, S., Mayol, E. and Fukasawa, M. (2011). Air-sea CO_2 fluxes along the coast of Chile: From CO_2 outgassing in central northern upwelling waters to CO_2 uptake in southern Patagonian fjords. *Journal of Geophysical Research, 116*(C9), C09006. doi:10.1029/2010JC006344

Visbeck, M.H., Hurrell, J.W., Polvani, L. and Cullen, H.M. (2001). The North Atlantic oscillation: past, present, and future. *Proceedings of the National Academy of Sciences USA, 98*, 12876–12877.

Visbeck, M., Chassignet, E. P., Curry, R. G., Delworth, T. L., Dickson, R. R. and Krahmann, G. (2003). 6 . The Ocean's Response to North Atlantic Oscillation Variability. *Atlantic*, *15*(8), 2581-2597. doi:10.1029/134GM06

Wanninkhof, R., Asher, W. E., Ho, D. T., Sweeney, C. and McGillis, W. R. (2009). Advances in Quantifying Air-Sea Gas Exchange and Environmental Forcing. *Annual Review of Marine Science*, *1*(1), 213-244. doi:10.1146/annurev.marine.010908.163742

Wanninkhof, R. (1992). Relationship between wind speed and gas exchange over the ocean. *Journal of Geophysical Research 97(C5)*:7373–7382.

Weiss, R. F. (1974). Carbon dioxide in water and seawater: the solubility of a non-ideal gas. *Marine Chemistry 2(3)*:203–215.

Weiss, R. F., and Price, B. A. (1980). Nitrous oxide solubility in water and seawater. *Marine Chemistry 8(4)*:347–359.

Williams, N. L., Juranek, L. W., Feely, R. A., Johnson, K. S., Sarmiento, J. L., Talley, L. D., Dickson, A.G., Gray, A.R., Wanninkhof, R., Russell, J.L., Riser, S.C. and Takeshita, Y. (2017). Calculating surface ocean pCO2from biogeochemical Argo floats equipped with pH: An uncertainty analysis. *Global Biogeochemical Cycles*, *31*(3), 591-604. doi:10.1002/2016GB005541

Wiltshire, K. H. and Manly, B. F. J. (2004). The warming trend at Helgoland Roads, North Sea: Phytoplankton response. *Helgoland Marine Research*, *58*(4), 269-273. doi:10.1007/s10152-004-0196-0

Winkler, L.W. (1888). Die Bestimmung des in Wasser gelösten Sauerstoffen. *Berichte der Deutschen Chemischen Gesellschaft, 21:* 2843–2855.

9. WEB REFERENCES

Ipcc.ch. (2018). Available at: https://www.ipcc.ch/pdf/assessmentreport/ar5/wg1/WGIAR5_SPM_brochure_en.pdf [Accessed 10 Jan. 2018].

Department of Commerce. (2018). NOAA Announces 2015 is Warmest Year on Record. [online] Available at: https://www.commerce.gov/news/blog/2016/01/noaa-announces-2015-warmest-year-record [Accessed 6 Mar. 2018].

Ncdc.noaa.gov. (2018). North Atlantic Oscillation (NAO) | Teleconnections | National Centers for Environmental Information (NCEI). [online] Available at: https://www.ncdc.noaa.gov/teleconnections/nao/ [Accessed 15 Jun. 2018].

Oceandata.sci.gsfc.nasa.gov. (2018). Oceancolor Data:/. [online] Available at: https://oceandata.sci.gsfc.nasa.gov/ [Accessed 15 May 2018].

Remss.com. (2018). Remote Sensing Systems. [online] Available at: http://www.remss.com/measurements/ccmp/ [Accessed 5 May 2018].

Science.oregonstate.edu. (2018). Ocean Productivity. Available at:

http://www.science.oregonstate.edu/ocean.productivity/ [Accessed 14 Jan. 2018].

Team, E. (2018). NOAA ESRL Global Monitoring Division. Retrieved from https://www.esrl.noaa.gov/gmd/